Lattice QCD form factor for $B_s \to D_s^* l\nu$ at zero recoil with nonperturbative current renormalization

E. McLean,[1,*] C. T. H. Davies,[1,†] A. T. Lytle,[2] and J. Koponen[3]

(HPQCD collaboration)[‡]

[1]*SUPA, School of Physics and Astronomy, University of Glasgow, Glasgow G12 8QQ, United Kingdom*
[2]*INFN, Sezione di Roma Tor Vergata, Via della Ricerca Scientifica 1, 00133 Roma RM, Italy*
[3]*High Energy Accelerator Research Organisation (KEK), Tsukuba 305-0801, Japan*

We present details of a lattice QCD calculation of the $B_s \to D_s^*$ axial form factor at zero recoil using the highly improved staggered quark (HISQ) formalism on the second-generation MILC gluon ensembles that include up, down, strange and charm quarks in the sea. Using the HISQ action for all valence quarks means that the lattice axial vector current that couples to the W can be renormalized fully nonperturbatively, giving a result free of the perturbative matching errors that previous lattice QCD calculations have had. We calculate correlation functions at three values of the lattice spacing, and multiple b-quark masses, for physical c and s. The functional dependence on the b-quark mass can be determined and compared to heavy quark effective theory expectations, and a result for the form factor obtained at the physical value of the b-quark mass. We find $\mathcal{F}^{B_s \to D_s^*}(1) = h^s_{A_1}(1) = 0.9020(96)_{\text{stat}}(90)_{\text{sys}}$. This is in agreement with earlier lattice QCD results, which use NRQCD b quarks, with a total uncertainty reduced by more than a factor of 2. We discuss implications of this result for the $B \to D^*$ axial form factor at zero recoil and for determinations of V_{cb}.

I. INTRODUCTION

The study of quark flavor-changing interactions is a key component of the search for physics beyond the standard model (SM). There are currently a number of related tensions between experimental measurements and SM predictions [1–19], along with discrepancies between systematically independent determinations of Cabibbo-Kobayashi-Maskawa (CKM) matrix elements [20–22]. A more precise understanding of these processes is needed to resolve these issues.

The $\bar{B}^0 \to D^{*+} \ell^- \bar{\nu}$ decay (and its charge conjugate, which we simply abbreviate to $B \to D^* \ell \nu$ from now on) supplies one of the three methods used for precisely determining the CKM element $|V_{cb}|$ [23–40]. Measurements of branching fractions are extrapolated through q^2 to the zero recoil point

to deduce $\mathcal{F}(1)|V_{cb}|$, where $\mathcal{F}(1)$ is the value of the only form factor contributing at zero recoil. Then a determination of $\mathcal{F}(1)$ in the standard model (via lattice QCD [39,41]) can be divided out to infer $|V_{cb}|$.

$|V_{cb}|$ is an important quantity and needs to be determined accurately. It constrains one side of the unitarity triangle via the ratio $|V_{ub}|/|V_{cb}|$. It is also a dominant uncertainty in the determination of the CP-violation parameter ϵ_K (where there is currently tension between the SM and experiment; see e.g., [42]).

Previous determinations of $|V_{cb}|$ have shown systematic discrepancies with each other. The two competing values were those derived from *exclusive* decays ($B \to D^* \ell \nu$ and $B \to D \ell \nu$ with $B \to D^*$ giving the more accurate result), and *inclusive* ($B \to X_c \ell \nu$, where X_c is any charmed hadronic state). In 2016 the Heavy Flavor Averaging Group (HFLAV) gave a value derived from exclusive $B \to D^*$ decays of $|V_{cb}|_{\text{excl}} = (39.05 \pm 0.47_{\text{exp}} \pm 0.58_{\text{th}}) \times 10^{-3}$ and from inclusive decays, using the kinetic scheme, of $|V_{cb}|_{\text{incl}} = (42.19 \pm 0.78) \times 10^{-3}$ [20]. It has since been suggested, based on unfolded Belle data [38], that the tension seen here arose (at least partly) from the use of a very constrained parametrization in the extrapolation of the experimental $B \to D^*$ decay rates to zero recoil [43–45].

---
*e.mclean.1@research.gla.ac.uk
†christine.davies@glasgow.ac.uk
‡http://www.physics.gla.ac.uk/HPQCD.

Recent exclusive determinations of V_{cb} have then used a less constrained parametrization to give a larger, and less precise, result for V_{cb} that is no longer in tension with the inclusive result. For example, the Particle Data Group quote $|V_{cb}|_{\text{excl}} = (41.9 \pm 2.0) \times 10^{-3}$ [46]. However, an even more recent V_{cb} determination from $B \to D^* \ell \nu$ data by the *BABAR* collaboration [47] used the less constrained parametrization but still found a tension with the inclusive result. This clearly points to the need for more work to improve the accuracy of the exclusive result. On the theory side a better understanding of the form factors for $B \to D^*$ from lattice QCD is required, both at zero recoil and away from zero recoil.

Another motivation for studying $B \to D^* \ell \nu$ is the tension between SM and experimental determinations of the ratio $R_{D^{(*)}} = \mathcal{B}(\bar{B} \to D^{(*)} \tau \bar{\nu}_\tau)/\mathcal{B}(\bar{B} \to D^{(*)} \ell \bar{\nu}_\ell)$ ($\ell = e$ or μ). The latest HFLAV report gives the combined statistical significance of the anomalies in R_D and R_{D^*} to be 3.8σ [20]. A preliminary new analysis from Belle [48], however, gives results closer to the SM and pulls the global average down to 3.1σ. More precise measurements and predictions will either confirm or dismiss a new physics explanation.

The weak decay process $B_s \to D_s^* \ell \nu$ is very similar to $B \to D^* \ell \nu$ and could also be used to determine $|V_{cb}|$ and test the SM. It is feasible to study this decay at the LHC and from the theoretical side it is a more attractive channel than $B \to D^*$. The absence of valence light quarks means that lattice QCD results have smaller statistical errors and are less computationally expensive. Finite-volume effects and the dependence on u/d quark masses (for quarks in the sea) are also smaller. The D_s^* has no Zweig-allowed strong decay mode, unlike the D^*, and is in fact a relatively long-lived particle [49] that can be considered "gold plated" in lattice QCD. This makes the $B_s \to D_s^* \ell \nu$ both a useful test bed for lattice techniques (that may be later used to study $B \to D^* \ell \nu$ decays) and a key decay process for which to make predictions ahead of experimental results.

Lattice QCD calculations have shown that several weak decay form factors are relatively insensitive to whether the spectator quark is a u/d or s quark [50–52]. A combination of chiral perturbation theory and heavy quark symmetry [53] backs up this expectation for B decays. We can therefore expect the form factors to be very similar for $B_s \to D_s^*$ and $B \to D^*$. A recent lattice calculation [41] found an insignificant $\mathcal{O}(1\%)$ difference at zero recoil: $\mathcal{F}^{B \to D^*}(1)/\mathcal{F}^{B_s \to D_s^*}(1) = 1.013(14)_{\text{stat}}(17)_{\text{sys}}$. Information from the study of $B_s \to D_s^*$ can then be applicable to $B \to D^*$.

Lattice QCD calculations of the $B_{(s)} \to D_{(s)}^*$ form factors at zero recoil have so far been performed by two collaborations using different methods. The Fermilab Lattice and MILC collaborations calculated $\mathcal{F}^{B \to D^*}(1)$ in [39,54] using the Fermilab action for both b and c quarks [55] and asqtad u/d quarks [56]. More recently the HPQCD collaboration

computed both $\mathcal{F}^{B \to D^*}(1)$ and $\mathcal{F}^{B_s \to D_s^*}(1)$ [41] using improved NRQCD b quarks [57,58] and highly improved staggered (HISQ) c and $u/d/s$ quarks [59]. The RBC/UKQCD [60] and LANL-SWME [61] collaborations are also working towards these form factors using variants of the Fermilab action for heavy quarks and JLQCD has a calculation in progress using Möbius domain-wall quarks [62].

The formalism to use for the heavy quarks is a major consideration in designing a lattice QCD calculation to determine these form factors. Most of the calculations discussed in the previous paragraph (apart from the JLQCD calculation) use approaches that make use of the nonrelativistic nature of heavy quark bound states to tune the b (and in some cases also c) quark masses. This avoids potentially large discretization effects appearing in the results in the form of a systematic error of size $(am_b)^n$, where n is an integer that depends on the level of improvement in the action. The absence of these discretization errors means that b quarks can be handled on relatively coarse lattices where $am_b > 1$. However the price to be paid is that the current operator that couples to the W boson is also implemented within a nonrelativistic framework and must then be renormalized to match the appropriate operator in continuum QCD. This matching can be done using perturbative lattice QCD but has only been done through $\mathcal{O}(\alpha_s)$ for these actions [63,64]. This leaves a substantial source of uncertainty from missing higher-order terms in the perturbative matching that is not easily reduced. This matching uncertainty contributes $\sim 80\%$ of the final error in the HPQCD calculation [41] and $\sim 30\%$ in the Fermilab/MILC calculation [39] because of the differing allowances for missing higher-order terms.

Here we report details and results of a calculation of the $B_s \to D_s^*$ form factor at zero recoil using an approach free of perturbative matching uncertainties. We perform our calculation on the second-generation MILC ensembles [65,66], including effects from $2 + 1 + 1$ flavors in the sea using the HISQ action. We also use the HISQ action for all valence quarks. We obtain results at a number of differing masses for the b (we refer to this generically as the *heavy quark h*), and perform an extrapolation to $m_h = m_b$. By using only HISQ quarks, we can obtain the normalizations of all required currents fully nonperturbatively. We refer to this as the *heavy-HISQ* approach. By using many heavy masses and multiple values of the lattice spacing, including very fine lattices, we can model both the form factor dependence on the heavy mass, and the discretization effects associated with using large am_h values.

The heavy-HISQ approach was developed by HPQCD to compute B meson masses and decay constants [67,68] and the b-quark mass [69,70]. It is also now being used by other collaborations for these calculations [71,72]. A proof-of-principle application of heavy HISQ to form factors was given in [73,74] for B_c decays, showing that the full q^2

range of the decay could be covered. Here we extend the approach to form factors for B_s decays but working only at zero recoil, a straightforward extension of earlier work. Using the heavy-HISQ approach also has the added benefit of elucidating the dependence of form factors on heavy quark masses, meaning that we can test expectations from heavy quark effective theory (HQET).

This article is structured in the following way: Sec. II defines the form factor and gives details of the lattice calculation, including the nonperturbative normalization and extrapolation in heavy quark mass; Sec. III presents our results and compares to earlier calculations, and Sec. IV gives our conclusions and outlook. In the Appendix, we give details of a number of tests we performed on the correlator fits and the continuum, chiral and heavy quark extrapolations.

II. CALCULATION DETAILS

A. Form factors

The differential decay rate for the $\bar{B}_s^0 \to D_s^{*+} l^- \bar{\nu}_l$ decay is given in the SM by

$$
\begin{aligned}
&\frac{d\Gamma}{dw}(\bar{B}_s^0 \to D_s^{*+} l^- \bar{\nu}_l) \\
&= \frac{G_F^2 M_{D_s^*}^3 |\bar{\eta}_{\text{EW}} V_{cb}|^2}{4\pi^3} \\
&\times (M_{B_s}^2 - M_{D_s^*}^2)\sqrt{w^2 - 1}\chi(w)|\mathcal{F}^{B_s \to D_s^*}(w)|^2, \quad (1)
\end{aligned}
$$

where $w = v_{B_s} \cdot v_{D_s^*}$, $v = p/M$ is the 4-velocity of each meson, and $\chi(w)$ is a known function of w with $\chi(1) = 1$ (see, e.g., Appendix G of [41]). $\bar{\eta}_{\text{EW}}$ accounts for electroweak corrections from diagrams where photons or Zs are exchanged in addition to a W^-, as well as the Coulomb attraction of the final-state charged particles [75–77]. The differential decay rate for the $B_s^0 \to D_s^{*-} l^+ \bar{\nu}_l$ is identical.

The form factor $\mathcal{F}^{B_s \to D_s^*}(w)$ is a linear combination of hadronic form factors that parametrize the vector and axial-vector matrix elements between initial and final-state

hadrons. A common choice of parametrization used in the context of HQET is [78]

$$
\langle D_s^*(\epsilon)|V^\mu|B_s\rangle = i\sqrt{M_{B_s}M_{D_s^*}}h_V^s(w)\epsilon_{\mu\nu\alpha\beta}\epsilon^{*\nu}v_{D_s^*}^\alpha v_{B_s}^\beta, \quad (2)
$$

$$
\begin{aligned}
\langle D_s^*(\epsilon)|A^\mu|B_s\rangle = \sqrt{M_{B_s}M_{D_s^*}}[&h_{A_1}^s(w)(w+1)\epsilon_\mu^* \\
&- h_{A_2}^s(w)\epsilon^* \cdot v_{B_s}v_{B_s\mu} - h_{A_3}^s(w)\epsilon^* \cdot v_{B_s}v_{D_s^*\mu}],
\end{aligned}
$$
$$(3)$$

where $V^\mu = \bar{c}\gamma^\mu b$ is the vector $b \to c$ current and $A^\mu = \bar{c}\gamma^\mu\gamma^5 b$ is the axial-vector current. ϵ is the polarization 4-vector of the D_s^* final state.

At zero recoil ($w = 1$), the vector matrix element vanishes, the axial-vector element simplifies to

$$
\langle D_s^*(\epsilon)|A^\mu|B_s\rangle = 2\sqrt{M_{B_s}M_{D_s^*}}h_{A_1}^s(1)\epsilon^{*\mu}, \quad (4)
$$

and $\mathcal{F}^{B_s \to D_s^*}(w)$ reduces to

$$
\mathcal{F}^{B_s \to D_s^*}(1) = h_{A_1}^s(1). \quad (5)
$$

Our goal is to compute $h_{A_1}^s(1)$.

All we need to do this is the matrix element $\langle D_s^*(\epsilon)|A^\mu|B_s\rangle$ with both the B_s and D_s^* at rest, with the D_s^* polarization ϵ in the same direction as the (spatial) axial-vector current.

B. Lattice calculation

The gluon field configurations that we use were generated by the MILC collaboration [65,66]. Table I gives the relevant parameters for the specific ensembles that we use. The gluon field is generated using a Symanzik-improved gluon action with coefficients calculated through $\mathcal{O}(\alpha_s a^2, n_f \alpha_s a^2)$ [79]. The configurations include the effect of $2 + 1 + 1$ flavors of dynamical quarks in the sea (u, d, s, c, with $m_u = m_d \equiv m_l$), using the HISQ action [59]. In three of the four ensembles (fine, superfine and ultrafine), the bare light quark mass is set to $m_{l0}/m_{s0} = 0.2$.

TABLE I. Parameters for the ensembles of gluon field configurations that we use [65,66]. a is the lattice spacing, determined from the Wilson flow parameter, w_0. Values for w_0/a are from set 1, [80], sets 2 and 3, [70] and set 4 [81]. The physical value of w_0 was determined at 0.1715(9) fm from f_π [82]. N_x is the spatial extent and N_t the temporal extent of the lattice in lattice units; n_{cfg} is the number of gluon field configurations in the ensemble and n_{src} the number of different time sources used per configuration. Light, strange and charm quarks are included in the sea, their masses are given in columns 6–8, and the valence quark masses in columns 9–11. The s and c valence quarks were tuned in [70]. We use a number of heavy quark masses to assist the extrapolation to the physical b mass. Column 12 gives the temporal separations between source and sink, T, of the three-point correlation functions computed on each ensemble.

Set	Handle	w_0/a	$N_x^3 \times N_t$	$n_{\text{cfg}} \times n_{\text{src}}$	am_{l0}	am_{s0}	am_{c0}	am_{s0}^{val}	am_{c0}^{val}	am_{h0}^{val}	T
1	Fine	1.9006(20)	$32^3 \times 96$	938×8	0.0074	0.037	0.440	0.0376	0.45	0.5, 0.65, 0.8	14,17,20
2	Fine physical	1.9518(7)	$64^3 \times 96$	284×4	0.0012	0.0363	0.432	0.036	0.433	0.5, 0.8	14,17,20
3	Superfine	2.896(6)	$48^3 \times 144$	250×8	0.0048	0.024	0.286	0.0234	0.274	0.427, 0.525, 0.65, 0.8	22,25,28
4	Ultrafine	3.892(12)	$64^3 \times 192$	249×4	0.00316	0.0158	0.188	0.0165	0.194	0.5, 0.65, 0.8	31,36,41

The fact that the m_{l0} value is unphysically high is expected to have only a small effect on $h_{A_1}^s(1)$, because there are no valence light quarks. The effect is quantified here by including a fourth ensemble (fine physical) with (approximately) physical m_{l0}.

We use a number of different masses for the valence heavy quark, h. This is in order to resolve the dependence of $h_{A_1}^s(1)$ on the heavy mass, so that an extrapolation to $m_h = m_b$ can be performed. By varying the heavy mass on each ensemble and by using ensembles at varying small lattice spacing, we can resolve both the discretization effects that grow with heavy quark mass ($am_{h0}^{val} \lesssim 1$) and the physical dependence of the continuum form factor on m_h.

Staggered quarks have no spin degrees of freedom (d.o.f.), so that a solution of the Dirac equation on each gluon field is numerically fast. The remnant of the doubling problem means that quark bilinears of specific spin parity have multiple copies, called "tastes" [59]. They differ in the amount of point splitting between the fields and the space-time dependent phase needed to substitute for the appropriate γ matrix. In this calculation we can use only local (nonpoint-split) bilinears, which is an advantage in terms of statistical noise, since no gluon fields are included in the current operator. In the standard staggered spin-taste notation, the operators that we use are pseudoscalar, $\Gamma_P = (\gamma^5 \otimes \gamma^5)$, vector, $\Gamma_V^\mu = (\gamma^\mu \otimes \gamma^\mu)$ and axial-vector, $\Gamma_A^\mu = (\gamma^\mu \gamma^5 \otimes \gamma^\mu \gamma^5)$.

We compute several two-point correlation functions on the ensembles detailed in Table I, combining HISQ propagators from solving the Dirac equation for each random wall time source. These correlation functions take the form

$$C_M(t) = \frac{1}{N_{\text{taste}}} \langle \Phi_M(t) \Phi_M^\dagger(0) \rangle,$$
$$\Phi_M(t) = \sum_{\mathbf{x}} \bar{q}(\mathbf{x}, t) \Gamma q'(\mathbf{x}, t), \qquad (6)$$

where $\langle \rangle$ represents a functional integral, q, q' are valence quark fields of the flavors the M meson is charged under, Γ is the spin-taste structure of M and $1/N_{\text{taste}}$ is the staggered quark normalization for closed loops. The random-wall source and the sum over $\mathbf{x}$ at the sink project onto zero spatial momentum. We compute the correlation functions for all t values, i.e., $0 \leq t \leq N_t$.

The correlation function for the heavy-strange pseudoscalar meson, H_s, with valence quark content $h\bar{s}$ and spin-taste structure Γ_P is constructed from HISQ propagators as

$$C_{H_s}(t) = \frac{1}{4} \sum_{\mathbf{x}, \mathbf{y}} \text{Tr}[g_h(x, y) g_s^\dagger(x, y)]. \qquad (7)$$

Here $g_q(x, y)$ is a HISQ propagator for flavor q, the trace is over color and $1/4$ is the staggered quark normalization.

$x_0 = 0$ and $y_0 = t$ and the sum is over spatial sites $\mathbf{x}$, $\mathbf{y}$. We also compute correlators for a charm-strange vector meson D_s^*, with structure Γ_V^i, using

$$C_{D_s^*}(t) = \frac{1}{4} \sum_{\mathbf{x}, \mathbf{y}} (-1)^{x_i + y_i} \text{Tr}[g_c(x, y) g_s^\dagger(x, y)]. \qquad (8)$$

We average over polarizations, $i = 1, 2, 3$.

We also compute correlation functions for two tastes of pseudoscalar heavy-charm mesons denoted H_c and $\hat{H}_c$ respectively. H_c has spin-taste structure Γ_P, and $\hat{H}_c$ has structure Γ_A^0. H_c correlators are computed using Eq. (7) (with g_s replaced with g_c), while $\hat{H}_c$ correlators are given by

$$C_{\hat{H}_c}(t) = \frac{1}{4} \sum_{\mathbf{x}, \mathbf{y}} (-1)^{\bar{x}_0 + \bar{y}_0} \text{Tr}[g_h(x, y) g_c^\dagger(x, y)], \qquad (9)$$

where we use the notation $\bar{z}_\mu = \sum_{\nu \neq \mu} z_\nu$. These correlators are used to normalize the axial vector $b\bar{c}$ current as discussed in Sec. II D.

A useful physical proxy (that does not run) for the quark mass is that of the pseudoscalar meson made from that flavor of quark. It is therefore also useful, for our heavy quark mass extrapolation, to calculate correlation functions for heavy-heavy pseudoscalars, denoted η_h, with spin-taste structure Γ_P using Eq. (7). Likewise, to test the impact of any mistuning of the charm and strange quark masses, we also determine η_c and η_s correlators analogously. We can tune the c and b masses using the experimental values for the η_c and η_b masses, allowing for slight shifts from missing QED effects and the fact that we do not allow these mesons to annihilate to gluons [69]. The mass of the η_s meson (which is not a physical state) can be fixed in lattice QCD from the K and π meson masses [82,83].

We then generate the three-point correlation functions that contain the H_s to D_s^* transition.

$$C_{3\text{pt}}(t, T) = \frac{1}{N_{\text{taste}}} \sum_{\mathbf{y}} \langle \Phi_{D_s^*}(T) A^i(\mathbf{y}, t) \Phi_{H_s}(0) \rangle,$$
$$A^\mu(\mathbf{y}, t) = \bar{c}(\mathbf{y}, t) \gamma^5 \gamma^\mu h(\mathbf{y}, t). \qquad (10)$$

Our H_s source is given spin taste Γ_P, the D_s^* sink, Γ_V^i, and the current insertion Γ_A^i. This gives the required cancellation of tastes within the three-point function [84]. In terms of HISQ propagators

$$C_{3\text{pt}}(t, T) = \frac{1}{4} \sum_{\mathbf{x}, \mathbf{y}, \mathbf{z}} (-1)^{\bar{y}_i + \bar{z}_i} \text{Tr}[g_h(x, y) g_c(y, z) g_s^\dagger(z, x)], \qquad (11)$$

where we fix $x_0 = 0$, $y_0 = t$ and $z_0 = T$. We compute the three-point correlation functions for all t values within $0 \leq t \leq T$, and $3T$ values that vary between ensembles and

are given in Table I. We average over the three directions for i for increased statistical precision.

C. Analysis of correlation functions

We use simultaneous Bayesian fits [85,86] to extract the axial-vector matrix element and meson masses from the two- and three-point correlation functions. This allows us to include the covariance between results at different heavy quark masses on a given ensemble into our subsequent fits in Sec. II E.

We fit the two-point correlation functions using the functional form

$$C_M(t)|_{\text{fit}} = \sum_n^{N_{\text{exp}}} (|a_n^M|^2 f(E_n^M, t)$$
$$- (-1)^t |a_n^{M,o}|^2 f(E_n^{M,o}, t)); \qquad (12)$$

$$f(E, t) = (e^{-Et} + e^{-E(N_t - t)}),$$

where N_t is the temporal extent of the lattice, and $E_n^{M,(o)}$, $a_n^{M,(o)}$ are fit parameters, with the excited-state energy parameters implemented as energy differences to the state below [85]. The second term accounts for the presence of opposite-parity states that contribute an oscillating term to the correlation function when using staggered quarks [59]. These terms do not appear when M is a pseudoscalar with a quark and antiquark of the same mass, so in the $M = \eta_h, \eta_c$, and η_s cases the second term is not required. For all correlator fits we set $N_{\text{exp}} = 5$; this allows the impact of systematic effects from excited states to be included in the ground-state parameters that we are interested in.

The three-point correlation functions have the fit form

$$C_{3\text{pt}}(t, T)|_{\text{fit}}$$
$$= \sum_{k,j=0}^{N_{\text{exp}}, N_{\text{exp}}} (a_j^{H_s} J_{jk}^{nn} a_k^{D_s^*} f(E^{H_s}, t) f(E_n^{D_s^*}, T - t)$$
$$+ a_j^{H_s,o} J_{jk}^{on} a_k^{D_s^*} (-1)^t f(E_n^{H_s,o}, t) f(E^{D_s^*}, T - t)$$
$$+ a_j^{H_s} J_{jk}^{no} a_k^{D_s^*,o} (-1)^{T-t} f(E^{H_s}, t) f(E_n^{D_s^*,o}, T - t)$$
$$+ a_j^{H_s,o} J_{jk}^{oo} a_k^{D_s^*,o} (-1)^T f(E_n^{H_s,o}, t) f(E^{D_s^*,o}, T - t)). \quad (13)$$

This includes fit parameters common to the fits of the H_s and D_s^* two-point correlators, along with new fit parameters J_{jk}.

We perform a single simultaneous fit containing each correlator computed (H_s, D_s^*, η_h, η_c, η_s, H_c, $\hat{H}_c$, and three-point) for each ensemble. We set Gaussian priors for the parameters J_{jk}, and log-normal priors for all other parameters. Using log-normal distributions forbids energy differences $E_{n+1}^M - E_n^M$ and amplitudes a_n^M (which can be

taken to be positive here) from moving too close to 0 or changing sign, improving stability of the fit.

Ground-state energies E_0^M are given priors of $(am_{q0} + am_{q'0} + a\Lambda_{\text{QCD}}) \pm 2a\Lambda_{\text{QCD}}$, where m_{q0} and $m_{q'0}$ are the masses of the appropriate quarks, and Λ_{QCD} is the confinement scale, which we set to 0.5 GeV. For $q = h$ or c, this corresponds to the leading order HQET expression for a heavy meson mass. Ground-state energies of oscillating states, $E_0^{M,o}$, are given priors of $(am_{q0} + am_{q'0} + 2a\Lambda_{\text{QCD}}) \pm 2a\Lambda_{\text{QCD}}$. Excited-state energy differences, $E_{i+1}^M - E_i^M$, $i > 0$ are given prior values $2a\Lambda_{\text{QCD}} \pm a\Lambda_{\text{QCD}}$. Priors for ground-state amplitudes a_0^M are set from plots of effective amplitudes. The resulting priors always have a variance at least ten times that of the final result for the ground state. We use log (amplitude) priors of $-1.20(67)$ for nonoscillating excited states and $-3.0(2.0)$ for oscillating excited states. The ground-state nonoscillating to nonoscillating three-point parameter, J_{00}^{nn}, is given a prior of 1 ± 0.6, and the rest of the three-point parameters J_{jk}^{nn} are given 0 ± 1.

$E_0^M = aM_M$ is the mass of the ground-state meson M in lattice units. The masses M_{H_s} and M_{η_h} can both be used as proxies for m_h in the extrapolation to $m_h = m_b$. The annihilation amplitude for an M meson is given (in lattice units) by

$$\langle 0 | \Phi_M | M \rangle|_{\text{lat}} = \sqrt{2M_M} a_0^M. \qquad (14)$$

The (as yet un-normalized) matrix element that we need to obtain $h_{A_1}^s(1)$ is given by

$$\langle D_s^*(\hat{k}) | A^k | H_s \rangle|_{\text{lat}} = 2\sqrt{M_{H_s} M_{D_s^*}} J_{00}^{nn}. \qquad (15)$$

To ensure that truncating the sum over states at N_{exp} accounts for the full systematic error from excited states, we cut out some data very close to the sources and sinks, where even higher excited states might have some effect. To do this we only include data with $t \geq t_{\text{cut}}$ and $t \leq N_t - t_{\text{cut}}$ in the two-point case and $t \leq T - t_{\text{cut}}$ in the three-point case. We can in principle use a different t_{cut} for every correlation function included in our fit, but we do not use a big range of t_{cut} values. They range from 1 to 3 for the three-point functions and up to 8 for the two-point functions.

The determination and minimization of the χ^2 function in our fit procedure requires the inversion of the covariance matrix that captures correlations between the different pieces of data (correlation functions) in our fit. The low eigenmodes of the correlation matrix are not well determined with the statistics that we have and so we implement a singular value decomposition (SVD) cut in the inversion of the correlation matrix to avoid underestimating the uncertainty in the parameters of the fit [86]. This replaces correlation matrix eigenvalues below λ_{min}, equal to svdcut times the largest eigenvalue, with λ_{min}. λ_{min} is estimated

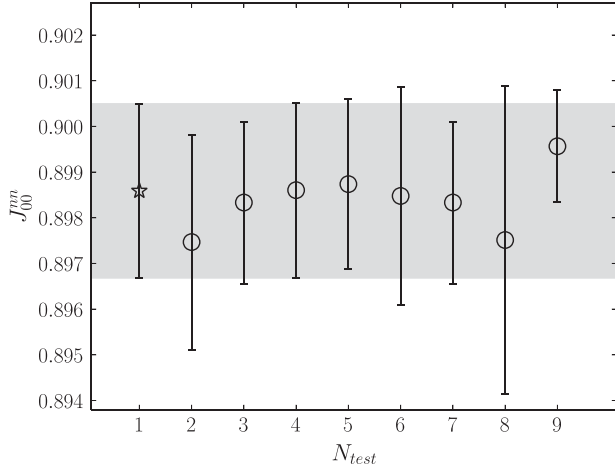FIG. 1. Tests of the stability of correlator fits for J_{00}^{nn} from fitting the two- and three-point correlators at heavy mass $am_{h0}^{\mathrm{val}} = 0.5$ on the fine ensemble. $N_{\mathrm{test}} = 1$ gives our final result. $N_{\mathrm{test}} = 2$ gives the results when all priors are broadened by 50%. $N_{\mathrm{test}} = 3$ and 4 give the results of setting $N_{\mathrm{exp}} = 4$ and 6, respectively. $N_{\mathrm{test}} = 5$, 6 give the result of setting $t_{\mathrm{cut}} = 2, 4$ respectively for all correlators. $N_{\mathrm{test}} = 7$ gives the result without marginalizing out the $n = 5$ excited state. $N_{\mathrm{test}} = 8$ gives the result of changing the SVD cut from 10^{-3} to 10^{-2}. $N_{\mathrm{test}} = 9$ gives the result from a fit containing only $am_{h0}^{\mathrm{val}} = 0.5$ correlators and hence with a smaller covariance matrix. This allows us, as a test, to use a reduced SVD cut of 10^{-5}.

using the diagnosis tools in the Corrfitter package [86] and corresponds typically to an svdcut of 10^{-3} here.

Figure 1 summarizes stability tests of our fits, focusing on the key parameter J_{00}^{nn} that is converted to the ground-state to ground-state transition amplitude using Eq. (15).

The fit parameters determined by our fits that we use to calculate the physical value for $h_{A_1}^{s}(1)$ are given in Table II. Notice that the statistical errors on the results grow with the

heavy quark mass. This is a well-understood problem in lattice heavy-light meson physics (see, e.g., [87]). Our method here has the advantage of including information from lighter-than-b heavy quarks with improved statistical precision.

D. Normalization of the axial current

The partially conserved axial-vector current for the HISQ action is a complicated linear combination of one-link and three-link lattice currents. In this study we use only local axial-vector currents. This simplifies the lattice QCD calculation but creates the need for our resulting current matrix element to be multiplied by a matching factor Z_A to produce the appropriate continuum current. We determine Z_A via a fully nonperturbative method [84].

We use the fact that the staggered local pseudoscalar current of spin taste ($\gamma^5 \otimes \gamma^5$), multiplied by the sum of its valence quark masses, is absolutely normalized via the PCAC relation. From the two-point H_c and $\hat{H}_c$ correlator fits we can extract the decay amplitudes $\langle 0|\bar{c}(\gamma^5 \otimes \gamma^5)h|H_c\rangle \equiv \langle 0|P|H_c\rangle$ and $\langle 0|\bar{c}(\gamma^0\gamma^5 \otimes \gamma^0\gamma^5)h|\hat{H}_c\rangle = \langle 0|A^0|\hat{H}_c\rangle$ as in Eq. (14). Then, the normalization for the local A^0 current (common to that of the local spatial axial-vector current A^k up to discretization effects), Z_A, is fixed by demanding that

$$(m_{h0}^{\mathrm{val}} + m_{c0}^{\mathrm{val}})\langle 0|P|H_c\rangle|_{\mathrm{lat}} = M_{\hat{H}_c} Z_A \langle 0|A^0|\hat{H}_c\rangle|_{\mathrm{lat}}. \quad (16)$$

The Z_A values found on each ensemble and am_{h0}^{val} are given in Table III.

There is an ambiguity in what mass to use on the right-hand side of Eq. (16). We use the non-Goldstone mass $M_{\hat{H}_c}$, but one could just as well replace this with M_{H_c} since the difference is a discretization effect. The meson mass difference is very small for heavy mesons [59], and so we

TABLE II. Values extracted from correlation function fits for $h_{A_1}^{s}(1)$, along with quantities required in our fits to determine a value at the physical point. Results are given on each gluon field ensemble for each valence heavy quark mass used. Results come from our simultaneous fits to two-point and three-point correlation functions: $h_{A_1}^{s}(1)$ values are determined using Eq. (19) and the ground-state meson masses in columns 4, 5, 6, 8, 9 and 10 from Eq. (12). f_{H_c} is the H_c meson decay constant determined from Eq. (A1).

Set	am_{h0}^{val}	$h_{A_1}^{s}(1)$	aM_{H_s}	$aM_{D_s^*}$	aM_{H_c}	af_{H_c}	aM_{η_h}	aM_{η_c}	aM_{η_s}
1	0.5	0.9255(20)	0.95972(12)	0.96616(44)	1.419515(41)	0.186299(70)	1.471675(38)	1.367014(40)	0.313886(75)
	0.65	0.9321(22)	1.12511(16)		1.573302(40)	0.197220(77)	1.775155(34)		
	0.8	0.9434(24)	1.28128(21)		1.721226(39)	0.207068(78)	2.064153(30)		
2	0.5	0.9231(21)	0.95462(12)	0.93976(42)	1.400034(28)	0.183472(62)	1.470095(25)	1.329291(27)	0.304826(52)
	0.8	0.9402(27)	1.27577(22)		1.702456(23)	0.203407(45)	2.062957(19)		
3	0.427	0.9107(46)	0.77453(24)	0.63589(49)	1.067224(46)	0.126564(70)	1.233585(41)	0.896806(48)	0.207073(96)
	0.525	0.9165(49)	0.88487(31)		1.172556(46)	0.130182(72)	1.439515(37)		
	0.65	0.9246(65)	1.02008(39)		1.303144(46)	0.133684(75)	1.693895(33)		
	0.8	0.9394(66)	1.17487(54)		1.454205(46)	0.137277(79)	1.987540(30)		
4	0.5	0.9143(51)	0.80245(24)	0.47164(39)	1.011660(32)	0.098970(52)	1.342639(65)	0.666586(89)	0.15412(17)
	0.65	0.9273(62)	0.96386(33)		1.169761(34)	0.100531(60)	1.650180(56)		
	0.8	0.9422(72)	1.11787(43)		1.321647(37)	0.101714(70)	1.945698(48)		

TABLE III. Normalization constants applied to the lattice axial vector current in (19). Z_A is found from (16) and $Z_{\rm disc}$ from (17).

Set	$am_{h0}^{\rm val}$	Z_A	$Z_{\rm disc}$
1	0.5	1.03178(57)	0.99819
	0.65	1.03740(58)	0.99635
	0.8	1.04368(56)	0.99305
2	0.5	1.03184(47)	0.99829
	0.8	1.04390(39)	0.99315
3	0.427	1.0141(12)	0.99931
	0.525	1.0172(12)	0.99859
	0.65	1.0214(12)	0.99697
	0.8	1.0275(12)	0.99367
4	0.5	1.00896(44)	0.99889
	0.65	1.01363(49)	0.99704
	0.8	1.01968(55)	0.99375

find the effect of changing the taste of meson mass used never exceeds 0.15% of Z_A throughout the range of ensembles and heavy masses that we use and has no impact on the continuum result.

We also remove tree-level mass-dependent discretization effects coming from the wave function renormalization [59] by multiplying by a factor $Z_{\rm disc}$. This is derived in [64] as

$$Z_{\rm disc} = \sqrt{\tilde{C}_h \tilde{C}_c},$$
$$\tilde{C}_q = \cosh am_{q,{\rm tree}}\left(1 - \frac{1 + \epsilon_{q,{\rm Naik}}}{2}\sinh^2 am_{q,{\rm tree}}\right). \quad (17)$$

See also [71]. $m_{q,{\rm tree}}$ is the tree-level pole mass in the HISQ action. It has an expansion in terms of the bare mass [59]

$$am_{q,{\rm tree}} = am_{q0}\left(1 - \frac{3}{80}am_{q0}^4 + \frac{23}{2240}am_{q0}^6\right.$$
$$\left. + \frac{1783}{537600}am_{q0}^8 - \frac{76943}{23654400}am_{q0}^{10} + \mathcal{O}(am_{q0}^{12})\right); \quad (18)$$

$\epsilon_{q,{\rm Naik}}$ fixes the Naik parameter [88] ($N = 1 + \epsilon$ is the coefficient of the tree-level improvement term for the derivative) in the HISQ action when it is being used for heavy quarks [59]. $\epsilon_{q,{\rm Naik}}$ is set to its tree-level value, removing the leading tree-level errors from the dispersion relation. As an expansion in $am_{q,{\rm tree}}$ it begins at $\mathcal{O}(am_{q,{\rm tree}})^2$ [59]. To determine $\epsilon_{q,{\rm Naik}}$ we use the closed form expression for it given in [64] and this can also be used along with Eq. (18) to evaluate $Z_{\rm disc}$. The pole condition can be used to show that the expansion of $\tilde{C}_q$ begins at am_{q0}^4 as $1 - 3am_{q0}^4/80 + \cdots$. The effect of $Z_{\rm disc}$ is then very small, never exceeding 0.2%. $Z_{\rm disc}$ values on each ensemble for each $am_{h0}^{\rm val}$ are given in Table III.

Combining these normalizations with the lattice current from the three-point fits, we find a value for the form factor at a given heavy mass and lattice spacing,

$$h_{A_1}^s(1) = \frac{1}{3}\sum_{k=1}^3 \frac{Z_A Z_{\rm disc}\langle D_s^*(\hat{k})|A^k|H_s\rangle|_{\rm lat}}{2\sqrt{M_{H_s}M_{D_s^*}}}. \quad (19)$$

E. Obtaining a result at the physical point

We now discuss how we fit our results for the zero recoil form factor, $h_{A_1}^s(1)$, as a function of valence heavy quark mass, sea light quark mass and lattice spacing to obtain a result at the physical point where the heavy quark mass is that of the b, the sea quark masses are physical and the lattice spacing is 0.

In summary, we fit our results for $h_{A_1}^s(1)$ to the following form:

$$h_{A_1}^s(1)(a, m_l, m_h) = 1 - \left(\frac{\varepsilon_c}{2}\right)^2 l_V + \varepsilon_c\varepsilon_h\frac{l_A}{2} - \left(\frac{\varepsilon_h}{2}\right)^2 l_P$$
$$+ \mathcal{N}_{\rm disc} + \mathcal{N}_{\rm mistuning}. \quad (20)$$

The terms in the first line allow for dependence on the valence heavy quark and charm quark masses (with $\varepsilon_q \equiv 1/m_q$) using input from HQET, to be discussed below. $\mathcal{N}_{\rm disc}$ and $\mathcal{N}_{\rm mistuning}$ account for discretization and mass mistuning effects, also discussed below. The physical result is then $h_{A_1}^s(1)(0, m_{l,{\rm phys}}, m_b)$.

1. Dependence on the heavy valence quark mass

Our fit of the m_h dependence is guided by HQET, which considers both the c quark and the heavy quark of mass m_h to be heavy here. In particular, for the parameter $h_{A_1}^{(s)}(1)$, HQET forbids terms of $\mathcal{O}(1/m_Q)$ where m_Q can be m_c or m_b [89]. The HQET expression for $h_{A_1}(1)$ is then given by [90,91]

$$h_{A_1}(1) = \eta_A\left(1 - \frac{l_V}{(2m_c)^2} + \frac{l_A}{2m_c m_h} - \frac{l_P}{(2m_h)^2}\right)$$
$$+ \mathcal{O}\left(\frac{1}{m_c^n m_h^m}, n + m \geq 3\right), \quad (21)$$

where l_V, l_A and l_P are $\mathcal{O}(\Lambda_{\rm QCD}^2)$ (with possible mild dependence on whether the spectator quark is s or u/d). η_A accounts for ultraviolet matching between HQET and QCD, and has been computed to two loops in perturbative QCD [92]. It has mild dependence on m_h through logarithms of m_c/m_h; at one-loop η_A has explicit form [93]

$$\eta_A = 1 - \frac{\alpha_s}{\pi}\left(\frac{1 + m_c/m_h}{1 - m_c/m_h}\ln\frac{m_c}{m_h} + \frac{8}{3}\right). \quad (22)$$

The coefficient of α_s/π then varies from -0.66 to -0.29 across the range of m_h from $m_h = m_c$ to $m_h = m_b$, taking $m_b/m_c = 4.577(8)$ [94]. The two-loop correction is small [92]. η_A is then close to 1 and differs by a few percent across our range of m_h.

Our calculation has results at multiple values of m_h, and could therefore in principle provide information on the coefficients l_A and l_P of the m_h-dependent terms in the HQET expansion. The charm quark mass is fixed to its physical value and so we cannot access the value of l_V independent of a choice of η_A at $m_h = m_c$. The terms in round brackets in Eq. (21), multiplying η_A, are all very small because of the suppression by heavy quark masses. To constrain them tightly requires very precise data and, as we see, we are not able to determine l_A, l_P or l_V accurately with our results. It therefore does not make sense to attempt to compare them accurately to HQET expectations. To do so would require using an appropriate quark mass definition [since different definitions will move quark mass dependence between the l_A term and the others in Eq. (21)] and the two-loop expression for η_A with appropriate value for α_s (since logarithmic m_h dependence of η_A can be misinterpreted as part of a polynomial in $1/m_h$).

Instead we simply take a HQET-inspired form for the m_h dependence and set η_A to 1, resulting in the first line of our fit form, Eq. (20). This is sufficient to test, through the results we obtain for l_A, l_V and l_P using this expression, that the HQET expectation for the approximate size of these coefficients is fulfilled. We take priors on $l_{A,V,P}$ in our fit of 0 ± 1 GeV^2.

We have several different proxies, derived from heavy meson masses, that we can take for the heavy quark mass that appears in ε_h in Eq. (20). We do not expect our physical result for $h^s_{A_1}$ to vary significantly depending on which meson mass we use, but the results for l_A, l_V and l_P vary because of different subleading terms in the relationship between meson and quark mass. The most obvious substitutions to use for the heavy quark mass are the mass of the pseudoscalar heavy-strange meson, M_{H_s}, and half the mass of the pseudoscalar heavyonium meson, M_{η_h}. We also tested using the quark mass in the minimal renormalon subtracted (MRS) scheme suggested in [95]. This takes

$$m_h = M_{H_s} - \bar{\Lambda}_{\text{MRS}} - \frac{\mu^2_{\text{MRS}}}{M_{H_s} - \bar{\Lambda}_{\text{MRS}}} + \mathcal{O}\left(\frac{1}{m^2_h}\right), \quad (23)$$

where $\mu^2_{\text{MRS}} = \mu^2_{\pi,\text{MRS}} - d_{H^{(*)}} \mu^2_{G,\text{MRS}}$ with $d_{H^{(*)}} = 1$ for pseudoscalar mesons and $-1/3$ for vectors. For this case we use parameters determined in [94] for the MRS scheme: $\bar{\Lambda}_{\text{MRS}} = 0.552(30)$ GeV, $\mu^2_{\pi,\text{MRS}} = 0.06(22)$ GeV^2 and $\mu^2_{G,\text{MRS}} = 0.38(1)$ GeV^2. We take m_h from Eq. (23) using our results for the mass of the pseudoscalar heavy-strange meson and m_c from our results for the mass of the D^*_s meson.

We take our central fit, for simplicity, from the result of using half the pseudoscalar heavyonium mass for m_h and half the pseudoscalar charmonium mass for m_c, i.e., taking

$$\varepsilon_q \equiv \frac{2}{M_{\eta_q}}. \quad (24)$$

We test the stability of the fit results under the different choices discussed above in Sec. III B.

2. Mistuning of other quark masses

Our calculation has results for multiple different heavy quark masses on each gluon field configuration. The valence charm and strange quark masses, however, are tuned to their physical values. This is done by fixing the η_c and η_s meson masses to their physical values in a pure QCD world allowing, for example, for η_c annihilation as discussed in [70]. Any possible mistuning of the charm quark mass is accounted for in our fit function by the dependence on the charm quark mass that is included in the first line of Eq. (20). When the fit function is evaluated at the physical point we set ε_c from the physical η_c mass.

The strange (valence and sea) and light (sea) mass mistunings are accounted for using the tuning in [70]. For the strange quark, we define $\delta_s = m_s - m^{\text{tuned}}_s$, where m^{tuned}_s is given by

$$m^{\text{tuned}}_s = m_{s0} \left(\frac{M^{\text{physical}}_{\eta_s}}{M_{\eta_s}}\right)^2. \quad (25)$$

$M^{\text{physical}}_{\eta_s}$ is determined in lattice simulations from the masses of the pion and kaon [82]. The ratio $\delta_s/m^{\text{tuned}}_s$ then gives the fractional mistuning. The valence strange quark masses are very well tuned, but the sea strange quark masses less so.

We similarly account for mistuning of the masses of the (sea) light quarks by defining $\delta_l = m_{l0} - m^{\text{tuned}}_l$. We find m^{tuned}_l from m^{tuned}_s, leveraging the fact that the ratio of quark masses is regularization independent, and the ratio was calculated in [71],

$$\left.\frac{m_s}{m_l}\right|_{\text{phys}} = 27.18(10). \quad (26)$$

We set m^{tuned}_l to m^{tuned}_s divided by this ratio.

The full term we include to account for mistuning is then given by

$$\mathcal{N}_{\text{mistuning}} = \frac{c^{\text{val}}_s \delta^{\text{val}}_s + c_s \delta_s + 2c_l \delta_l}{10 m^{\text{tuned}}_s}, \quad (27)$$

where c_l, c_s and c^{val}_s are fit parameters with prior distributions 0 ± 1. We neglect $\delta^2_{s,l}$ contributions since these are

an order of magnitude smaller and are not resolved in the results of our lattice calculation.

The gluon field configurations that we use have $m_u = m_d \equiv m_l$ in the sea. In the real world this is not true. We test the impact of possible isospin breaking on our fits by testing for sensitivity to the sea light quark masses. We do this by changing the m_l^{tuned} value up and down by the expected value for $m_d - m_u$ [46]. We find the effect to be completely negligible in comparison to the other sources of error.

3. Discretization effects

Discretization effects in our lattice QCD results are accounted for following the methodology of [68]. We take

$$\mathcal{N}_{\text{disc}} = \sum_{i=0, j+k\neq 0}^{2,2,2} d_{ijk} \left(\frac{2\Lambda_{\text{QCD}}}{M_{\eta_h}}\right)^i \left(\frac{am_{h0}^{\text{val}}}{\pi}\right)^{2j} \left(\frac{am_{c0}^{\text{val}}}{\pi}\right)^{2k}. \tag{28}$$

The leading terms, with $i = 0$, allow for discretization effects that are set by the heavy quark mass and also discretization effects that are set by the charm quark mass (or indeed any other lighter scale that is independent of heavy quark mass). The $i > 0$ terms allow for discretization effects to vary as the heavy quark mass is varied, with M_{η_h} being used here as a proxy for the heavy quark mass. d_{ijk} are fit parameters with prior distributions 0 ± 1.0. All discretization effects are of even order by construction of the HISQ action [59].

We tested the impact on the fit of including extra discretization effects set by the scale Λ_{QCD} but this made no difference (since such effects are much smaller than those already included by the am_{c0}^{val} terms). We also tested the effects of increasing the number of terms in each sum, but the final result remained unchanged.

4. Finite-volume effects

The finite volume effects in our lattice results are expected to be negligible, because we are working with heavy mesons that have no valence light quarks and no Zweig-allowed strong decay modes. Coupling to chiral loops or decay channels with pions that could produce significant finite-volume effects [96] is therefore absent and we can safely ignore finite-volume effects here.

In Sec. III B we detail the results of several tests of the stability of our final result under changes to the details of the fit.

5. Topological charge effects

It has been observed that the finest MILC ensembles ($a \simeq 0.45$ fm and finer) suffer from slow variation in the topological charge [97] with Monte Carlo time. The question then arises if physical observables obtained by averaging over the ensemble could be biased by being measured in only a small range of topological charge

sectors. This issue is addressed in [97] through a calculation of the "topological adjustment" needed for meson masses and decay constants on the ultrafine lattices used here (with $m_l/m_s = 0.2$). The adjustment found for the D_s decay constant is 0.002%. We might expect the impact of a frozen topological charge on $h_{A_1}^s(1)$ to be of a similar size to this, given that it involves a transition between heavy-strange mesons. Allowing for this systematic uncertainty (or even ten times it) has a negligible effect on our final result.

III. RESULTS AND DISCUSSION

A. Result for $h_{A_1}^s(1)$

The results of our correlation function fits (discussed in Sec. II C) are given in Table II. We tabulate values for $h_{A_1}^s(1)$ at each heavy quark mass that we have used on each gluon field ensemble from Table I. We also tabulate the meson masses needed to allow determination of $h_{A_1}^s(1)$ at the physical point, using the fit form of Eq. (20).

The fit function of Eq. (20) is readily applied, giving a $\chi^2/[\text{dof}]$ of 0.21 for 12 d.o.f. Figure 2 shows our results for $h_{A_1}^s(1)$ along with the fit function at zero lattice spacing and physical u/d, s and c quark masses as the grey band. Evaluating the fit function at the physical b mass, as determined by M_{η_b}, gives our final result

$$\mathcal{F}^{B_s \rightarrow D_s^*}(1) = h_{A_1}^s(1) = 0.9020(96)_{\text{stat}}(90)_{\text{sys}}. \tag{29}$$

Adding the statistical and systematic errors in quadrature, we find a total fractional error of 1.5%. The error budget for
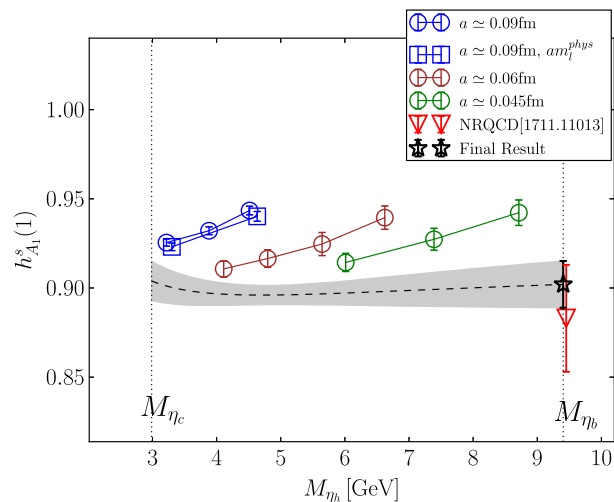

FIG. 2. $h_{A_1}^s(1)$ against M_{η_h} (a proxy for the heavy quark mass). The grey band shows the result of the extrapolation to $a = 0$ at physical l, s and c masses; the black star shows our result at the physical b-quark mass. Gluon field ensembles listed in the legend follow the order of sets in Table I. Solid lines simply join the points on a given ensemble for added clarity. The red inverted triangle gives the determination of the same quantity from a previous study using the NRQCD action for the b quark [41].

TABLE IV. Error budget for $h_{A_1}^s(1)$. Errors are given as a percentage of the final answer. The mass mistuning error includes that from valence strange and sea light and strange quarks; we find that taking a ± 10 MeV uncertainty in the physical value of the η_b mass has a negligible effect.

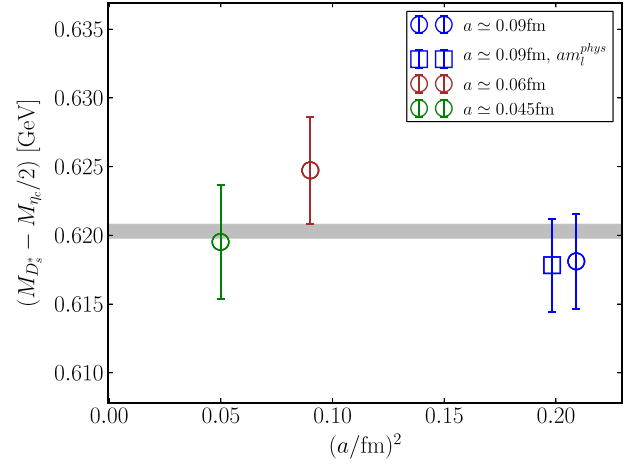| Source	% Fractional error
Statistics $+Z_A$	1.06
$a \to 0$	0.73
$m_h \to m_b$	0.69
Mass mistuning	0.20
Total	1.45

FIG. 3. The D_s^* meson mass obtained on each of our gluon field ensembles, given as a difference from one half the η_c meson mass. Errors include statistical and lattice spacing uncertainties. The grey band gives the experimental result [46].

this result is given in Table IV. Note that we allow for an additional ± 10 MeV uncertainty in the physical value of the η_b mass beyond the experimental uncertainty, since our lattice QCD results do not include the effect of η_b annihilation and QED [68]. This has no effect, however, since the heavy quark mass dependence is so mild.

Our total uncertainty is dominated by the statistical errors in our lattice results. The systematic error is dominated by that from the continuum extrapolation.

We include in Fig. 2 the value from the only other lattice determination of $h_{A_1}^s(1)$ [41]. This calculation also used MILC $n_f = 2 + 1 + 1$ gluon field ensembles, but with the bulk of the ensembles used having coarser lattice spacing. This was made possible by the use of the NRQCD action for the b quark [58]. The HISQ action was used for all the other quarks. The result of this calculation was $h_{A_1}^s(1) = 0.883(12)_{\text{stat}}(28)_{\text{sys}}$. Our result is in agreement with this, but with substantially smaller errors. The NRQCD uncertainty of 3.4% is dominated by the systematic error from the $\mathcal{O}(\alpha_s)$ matching factor used to normalize the NRQCD-HISQ current and this error is absent from our calculation.

In addition to a value for $h_{A_1}^s(1)$ our calculation is able to give information on the physical dependence on the heavy quark mass of $\mathcal{F}^{H_s \to D_s^*}(1)$. We see from Fig. 2 that this dependence is very mild to the point of being absent. We can determine the ratio of $\mathcal{F}^{H_s \to D_s^*}(1)$ for $m_h = m_b$ to $m_h = m_c$ (albeit that this latter point corresponds to an unphysical $D_s \to D_s^*$ decay) and find the value 0.998(23). Each of the terms (including η_A) in the HQET expectation of Eq. (21) can give effects of the order of a few percent to this ratio. The fact that we find no heavy quark mass dependence at the level of 2% shows that these effects must tend to cancel out.

The fit of our lattice results to Eq. (20) gives fit parameters $l_{V,A,P}$ which, as discussed in Sec. II E 1, provide a test of HQET. We find

$$l_V^s = 0.71(28) \text{ GeV}^2,$$
$$l_A^s = -0.34(32) \text{ GeV}^2,$$
$$l_P^s = -0.53(34) \text{ GeV}^2, \tag{30}$$

from our baseline fit. These results are compatible with values of $\mathcal{O}(\Lambda_{\text{QCD}}^2)$ as expected by HQET. As discussed in Sec. II E 1 these fit parameters change depending on the proxy that we use for the quark mass as well as our treatment of η_A. However, as we show in the tests performed in the next section (see Fig. 5) this has little impact on our value for $h_{A_1}^s(1)$.

B. Further tests of our fit

Because we tune our b and c valence quark masses using the pseudoscalar heavyonium meson mass, we can independently test our results by comparing both our heavy-strange and D_s^* meson masses against experiment. These results are shown in Figs. 3 and 4. In each case we subtract half the corresponding pseudoscalar heavyonium mass to reduce lattice spacing uncertainties in the comparison to experiment [87].

Figure 3 shows that our D_s^* meson mass agrees with experiment on all our ensembles at the level of our 5 MeV uncertainties. Systematic effects from missing QED and η_c annihilation are expected to be of size a few MeV [87].

Figure 4 shows our results for the heavy-strange pseudoscalar meson mass as a function of the pseudoscalar heavyonium mass. We show the difference $\Delta_h = M_{H_s} - M_{\eta_h}/2$ to remove the leading m_h dependence and also to reduce uncertainties from the value of the lattice spacing. We fit Δ_h to a simple function of ε_h [Eq. (24)],

$$\Delta_h(a, m_l, m_h) = \left(\sum_{i=-1}^{i=1} c_i \varepsilon_h^i \right) (1 + \mathcal{N}_{\text{disc}} + \mathcal{N}_{\text{mistuning}}). \tag{31}$$

The leading, linear, term in ε_h allows for the fact that the heavyonium (η_h) binding energy grows linearly with m_h in
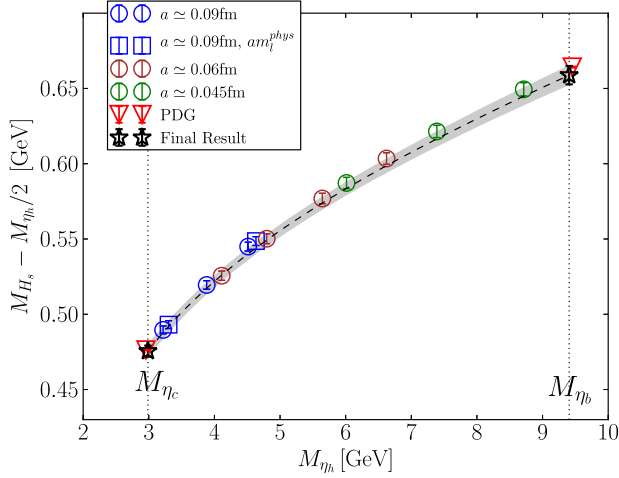
FIG. 4. The H_s meson mass obtained on each of our gluon field ensembles, given as a difference to one half of the η_h meson mass. Errors include statistical and lattice spacing uncertainties. The grey band gives a fit to the heavy-quark mass dependence as discussed in the text, with black stars giving our results at $m_h = m_c$ and $m_h = m_b$. The inverted red triangles give the corresponding experimental values [46].

a $1/r$ potential. We take priors on the c_i of c_{-1}:0.05(5); c_0:0.5(5); c_1:0(1). $\mathcal{N}_{\rm disc}$ takes the same form as in Eq. (28) with $a\Lambda_{\rm QCD}$ (where $\Lambda_{\rm QCD}$ is taken as 0.5 GeV) replacing $am_{c0}^{\rm val}$, which is not relevant here. $\mathcal{N}_{\rm mistuning}$ takes the same form as in Eq. (27).

Our result for the difference $M_{H_s} - M_{\eta_h}/2$ in the continuum at $m_h = m_c$ is 0.4755(37) GeV and at $m_h = m_b$ is 0.6588(61) GeV. These agree well with the earlier HPQCD results on $n_f = 2 + 1$ gluon field configurations of 0.4753(22) GeV [87] and 0.658(11) GeV [67]. They also agree well with the experimental values of 0.4764(3) GeV and 0.6674(12) GeV [46], allowing for the $\sim$3–5 MeV effect from missing QED and η_b and η_c annihilation processes in the lattice QCD results.

We also performed a number of tests of our continuum/ heavy-quark mass dependence fit to our results for $h_{A_1}^s(1)$. These are tabulated graphically in Fig. 5.

One of the tests, denoted ratio with f_{H_c} in Fig. 5, is described in more detail in Appendix A. It involves fitting the ratio of $h_{A_1}^s(1)$ to the H_c decay constant, as a function of heavy quark mass and, after determining the continuum result at $m_h = m_b$, multiplying by the value for the B_c decay constant determined from lattice QCD to obtain $h_{A_1}^s(1)$. The reason for doing this is because this ratio has smaller discretization effects than $h_{A_1}^s(1)$ alone, as is clear from Fig. 8 in Appendix A. It has stronger dependence on m_h, however, coming from the H_c decay constant, along with sizeable uncertainties introduced from the uncertainty in the lattice spacing. Another disadvantage is that the physical result for H_c decay constant must also be obtained. We find that this method gives results in agreement with our
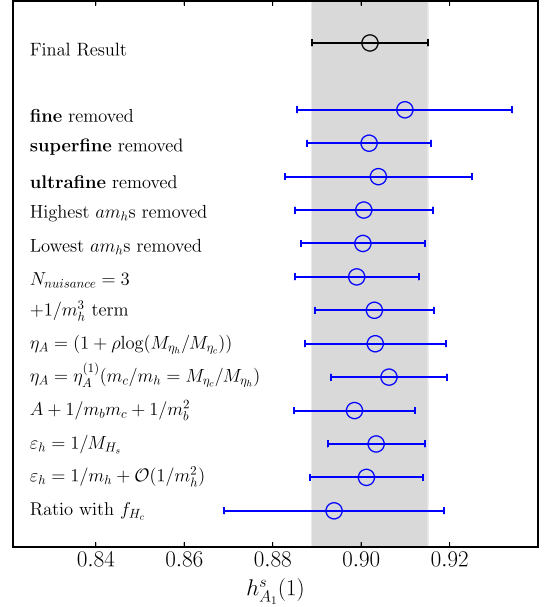

FIG. 5. Results of testing the fit to $h_{A_1}^s(1)$ results. The top black point gives our baseline fit result in the continuum and at physical b-quark mass. The top three blue points show the corresponding value if results from the fine, superfine or ultrafine ensembles are dropped from the fit. The fourth and fifth blue points show the result if instead results at the highest/lowest $am_{h0}^{\rm val}$ value on each ensemble are removed. $N_{\rm nuisance} = 3$ shows the result of truncating each sum in $\mathcal{N}_{\rm disc}$ (28) at 3 rather than 2. $+ 1/m_h^3$ results from adding an extra term to (20) of the form $p/M_{\eta_h}^3$ where p is a fit parameter with the same prior as $l_{V,A,P}^s$. In this case the Bayes factor falls by a factor of 7, suggesting that the results do not contain a cubic dependence on the heavy mass. The next two points show the results of including specific implementations of η_A described in Sec. II E (rather than the value 1). In the upper variant parameter ρ is given prior 0 ± 1. The lower variant shows the result of using the one-loop expression for η_A [Eq. (22)], with m_c/m_h replaced with M_{η_c}/M_{η_h}. $A + 1/m_b m_c + 1/m_b^2$ is the result of replacing $1 + l_V/m_c^2$ in the fit with a fit parameter A with prior distribution 1 ± 1. The fact that this does not affect the fit shows that mistuning of the charm quark mass is a negligible effect here. The points with labels beginning $\varepsilon_h =$ show the result of replacing the heavy mass proxy $M_{\eta_h}/2$ with M_{H_s} and the MRS quark mass [Eq. (23)], respectively. The bottom point labeled ratio with f_{H_c} is the result of an alternative extrapolation described in Appendix A.

standard fit but with significantly larger uncertainties. It provides a good test, however, because it has very different m_h dependence.

C. Implications for $B \to D^*$

As discussed in Sec. I, $h_{A_1}^s(1)$ is expected to be close in value to the equivalent $B \to D^*$ form factor, since they only differ in the mass of the light spectator quark and in effects arising from the strong decay of the D^* to $D\pi$. In [41] the ratio of the two form factors was found to be
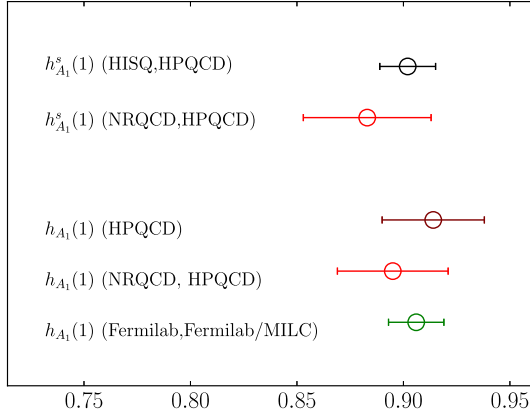
FIG. 6. Comparison of lattice QCD results for $h^s_{A_1}(1)$ and $h_{A_1}(1)$. Our results for $h^{(s)}_{A_1}(1)$ are marked (HISQ, HPQCD) and for $h_{A_1}(1)$ are marked (HPQCD). Those marked (NRQCD, HPQCD) are from [41] and the value marked (Fermilab, Fermilab/MILC) is from [39].

$h_{A_1}(1)/h^s_{A_1}(1) = 1.013(14)_{\text{stat}}(17)_{\text{sys}}$. Note that systematic effects from the perturbative matching of the NRQCD-HISQ current largely cancel in this ratio.

Multiplying this by our result for $h^s_{A_1}(1)$, we can determine $h_{A_1}(1)$ as

$$\mathcal{F}^{B \to D^*}(1) = h_{A_1}(1) = 0.914(24), \qquad (32)$$

adding all the uncertainties in quadrature.

In Figs. 6 and 7, we compare current lattice results for $h_{A_1}(1)$ and $h^s_{A_1}(1)$. Figure 6 compares final results for $h^s_{A_1}(1)$ from the HPQCD calculation using NRQCD b quarks and HISQ lighter quarks [41] with our full HISQ result given here [Eq. (29)]. It also compares final results for $h_{A_1}(1)$ from using the Fermilab approch [39] for b and c quarks and asqtad light quarks, NRQCD b quarks and HISQ lighter quarks [41] and our result from Eq. (32) using the strange to light ratio from [41]. Good agreement between all results is seen, well within the uncertainties quoted.

In Fig. 7, we show more detail of the comparison by plotting the lattice results from the previous Fermilab/MILC [39] and NRQCD b [41] calculations as a function of the valence spectator light quark mass (given by the square of the pion mass). Note that, for the results for $h_{A_1}(1)$ to the left of the plot, the valence light and sea masses are the same. For the $h^s_{A_1}(1)$ points from [41] to the right of the plot, the sea light (along with s and c) quark masses take their physical values. Although agreement for $h_{A_1}(1)$ is seen at physical light quark mass in the continuum limit from all approaches, the NRQCD-HISQ results show systematic light quark mass dependence away from this point that is not visible in the Fermilab/MILC results.
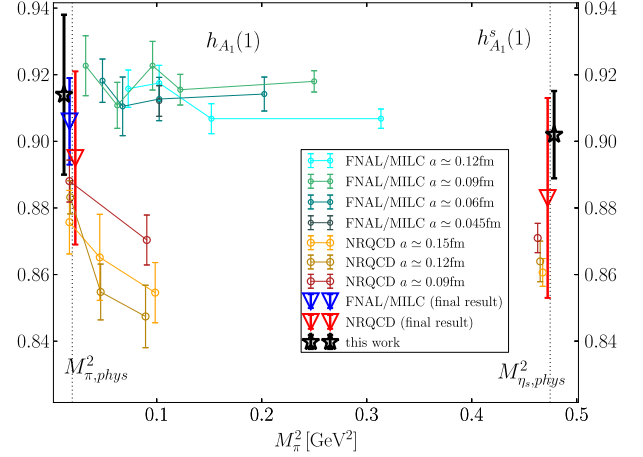
FIG. 7. More detailed comparison of lattice QCD results for $h_{A_1}(1)$ (left side) and $h^s_{A_1}(1)$ (right side). Raw results for $h_{A_1}(1)$ are from [41] and [39] and are plotted as a function of valence ($=$ sea) light quark mass, given by the square of M_π. On the right are points for $h^s_{A_1}(1)$ from [41] plotted at the appropriate valence mass for the s quark, but obtained at physical sea light quark masses. The final result for $h_{A_1}(1)$ from [39], with its full error bar, is given by the inverted blue triangle. The inverted red triangles give the final results for $h_{A_1}(1)$ and $h^s_{A_1}(1)$ from [41]. Our results here are given by the black stars.

The two sets of results move apart as the spectator quark mass increases, and it is therefore not clear how well they would agree for spectator s quarks.

Our results, shown in Fig. 7 with black stars, agree with the NRQCD-HISQ results for $h^s_{A_1}(1)$. The smaller uncertainties from using a fully nonperturbative current normalization here show that the perturbative matching uncertainty allowed for in [41] was conservative. Using the s/l ratio from this calculation, where the perturbative matching uncertainty cancels, allows us to obtain an $h_{A_1}(1)$ result that agrees well with both earlier values. Our uncertainty on $h_{A_1}(1)$ is similar to that from [41] once we have combined the uncertainty from the ratio with that from our value for $h^s_{A_1}(1)$. However we have removed the perturbative matching uncertainty that dominates the NRQCD-HISQ error.

IV. CONCLUSIONS

We have calculated the form factor at zero recoil, $\mathcal{F}^{B_s \to D^*_s}(1)$ or $h^s_{A_1}(1)$, using the relativistic HISQ formalism in full lattice QCD. This allows us to normalize the $b \to c$ current fully nonperturbatively for the first time and to determine how the form factor depends on the heavy quark mass (at physical charm quark mass). Our results show that dependence on the heavy quark mass is very mild (see Fig. 2).

Our result

$$\mathcal{F}^{B_s \to D^*_s}(1) = h^s_{A_1}(1) = 0.9020(96)_{\text{stat}}(90)_{\text{sys}} \qquad (33)$$

agrees with an earlier lattice QCD result [41], but with half the uncertainty because of the nonperturbative normalization of the current. Using the strange to light quark ratio from the earlier paper we are able to obtain a result for $\mathcal{F}^{B \to D^*}(1)$,

$$\mathcal{F}^{B \to D^*}(1) = h_{A_1}(1) = 0.914(24), \qquad (34)$$

which is also free of perturbative matching uncertainties.

$h_{A_1}^s(1)$ will be a useful value to compare to experimental results in future to determine V_{cb}. It has some advantages from a lattice QCD perspective over h_{A_1} as discussed in Sec. I. However, $h_{A_1}(1)$ can be combined with existing experimental results to obtain a value for the CKM element V_{cb}. The method of combination has been questioned recently when it was realized that the HQET constraints on the extrapolation of the exclusive experimental data to the zero recoil point were having a significant effect. Loosening these constraints gives a higher, but less precise, value for the combination $|\bar{\eta}_{EW} V_{cb}| h_{A_1}(1)$ (see, for example, the V_{ub}/V_{cb} minireview in [46]). Combining this experimental value with lattice QCD results for $h_{A_1}(1)$ then gives a result for V_{cb} from the $B \to D^* \ell \nu$ exclusive decay that agrees with, but is less accurate than, that from inclusive $b \to c$ decays. We do not convert our h_{A_1} result into a value for V_{cb} here since it is clear from Fig. 6 that we agree with existing results (such as that in [41]) and, on its own, our new result does not have sufficient accuracy to reduce uncertainties in V_{cb}.

In future lattice QCD form factor calculations for both $B_s \to D_s^*$ and $B \to D^*$ need to work away from zero recoil to improve overlap with experimental results without the need for extrapolation.[1] Our results here demonstrate the efficacy of HPQCD's heavy-HISQ approach for form factors at zero recoil. Away from zero recoil we expect it to be even more useful because it is possible to map out the full q^2 range of the decay [73], where nonrelativistic approaches must stay close to zero recoil because of systematic errors that grow with the magnitude of the daughter meson momentum. Heavy HISQ calculations are underway for the form factors for $B_{(s)} \to D_{(s)}^*$, $B_c \to J/\psi$ decay, and the related $B_s \to D_s$ decay over the full q^2 range, using the techniques developed for $c \to s$ decays to normalize the currents nonperturbatively [51,84]. Initial results [74,99] look very promising.

ACKNOWLEDGMENTS

APPENDIX: RATIO METHOD FOR DETERMINING $h_{A_1}^s(1)$

It turns out that the significant discretization effects visible in our results for $h_{A_1}^s(1)$ (Fig. 2) are largely canceled when we divide them by lattice QCD results for the decay constant of the heavy-charm pseudoscalar meson, f_{H_c}. This was also observed in [74] for vector form factors involving a $b\bar{c}$ current. f_{H_c} is determined from the matrix element between the vacuum and the H_c meson of the temporal axial-vector $b\bar{c}$ current, whereas $h_{A_1}^s(1)$ is the matrix element between the H_s and D_s^* mesons of the spatial axial vector $b\bar{c}$ current. They behave very differently as a function of heavy quark mass but in practice have similar discretization errors (compare Figs. 2 and 9). We can make
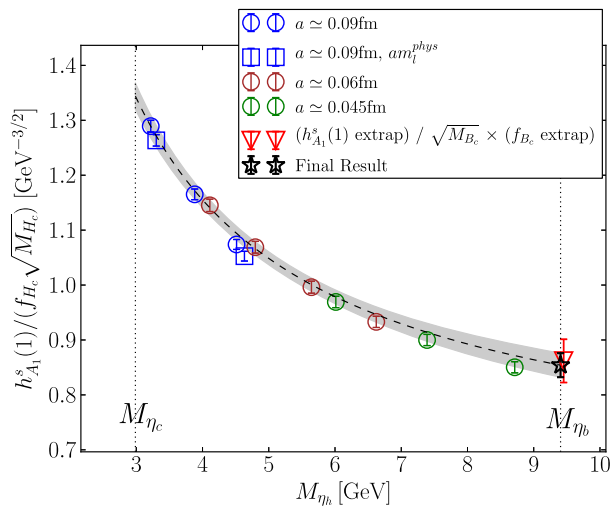

FIG. 8. The ratio $h_{A_1}^s(1)/(f_{H_c}\sqrt{M_{H_c}})$ plotted against M_{η_h} (a proxy for the heavy quark mass). Gluon field ensembles listed in the legend follow the order of sets in Table I. The grey band shows the result of the fit described in the text, evaluated at $a = 0$ and physical l, s and c quark masses to give the physical heavy quark mass dependence of the ratio. At $m_h = m_b$ we obtain the result given by the black star. For comparison with our previous fit for $h_{A_1}^s(1)$ the inverted red triangle shows our result from Eq. (33) converted to a ratio using the value for f_{B_c} from Fig. 9 and M_{B_c} from experiment [46].
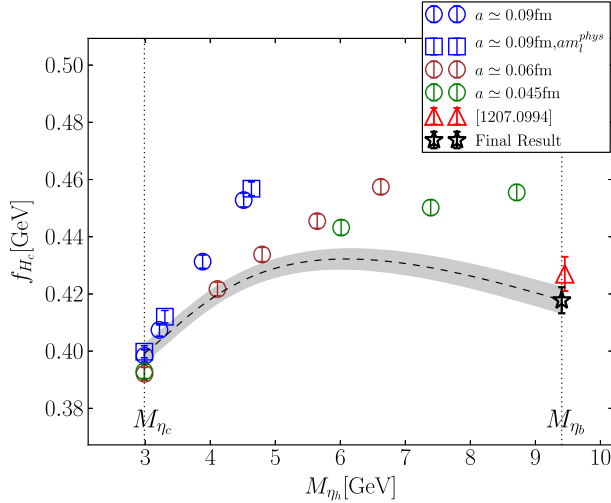
FIG. 9. The heavy-charm pseudoscalar meson decay constant, f_{H_c}, plotted against M_{η_h} (a proxy for the heavy quark mass). Gluon field ensembles listed in the legend follow the order of sets in Table I. The grey band shows the result of the fit described in the text, evaluated at $a = 0$ and physical l, s and c quark masses to give the physical heavy quark mass dependence of the decay constant. At $m_h = m_b$ we obtain the result given by the black star. The red triangle shows the result from a previous heavy-HISQ determination of f_{B_c} on $n_f = 2 + 1$ gluon field ensembles [68].

use of this in fitting the heavy quark mass dependence of their ratio with reduced discretization effects. We also then need to fit the H_c decay constant on its own in order to determine a physical value for the B_c that we can use to determine $h_{A_1}^s(1)$ at the physical point.

f_{H_c} is found using the PCAC relation for HISQ quarks

$$f_{H_c} = \frac{m_{h0} + m_{c0}}{M_{H_c}^2} \langle 0|P|H_c\rangle|_{\text{lat}}, \qquad (A1)$$

where $\langle 0|P|H_c\rangle$ is determined in the fit to the H_c two-point correlation functions via (14). We use a pseudoscalar operator, P, with spin-taste $\gamma_5 \otimes \gamma_5$ so f_{H_c} is absolutely normalized. Results for f_{H_c} for each ensemble are given in Table II and plotted in Fig. 9.

On each ensemble, at each heavy quark mass, we form the ratio $h_{A_1}^s(1)/(f_{H_c}\sqrt{M_{H_c}})$, plotted in Fig. 8. Although discretization effects largely cancel, the ratio varies strongly with changing heavy quark mass. This makes fitting this ratio as a function of heavy quark mass and lattice spacing very different to that of $h_{A_1}^s(1)$, with different systematic effects.

We use a fit function of the same form for both $h_{A_1}^s(1)/(f_{H_c}\sqrt{M_{H_c}})$ and f_{H_c}. Denoting the quantity being fit by F, we write (following [68])

$$F(a, m_h, m_l) = A\left(\frac{\alpha_s(M_{\eta_h}/2)}{\alpha_s(M_{\eta_c}/2)}\right)^p M_{\eta_h}^{n/2}$$
$$\times \sum_{i,j,k=0}^{2,2,2} d_{ijk}\left(\frac{2\,\text{GeV}}{M_{\eta_h}}\right)^i \left(\frac{am_{h0}^{\text{val}}}{\pi}\right)^{2j} \left(\frac{am_{c0}^{\text{val}}}{\pi}\right)^{2k}$$
$$\times \left(1 + \mathcal{N}_{\text{mistuning}} + c_c\frac{M_{\eta_c} - M_{\eta_c}^{\text{physical}}}{M_{\eta_c}^{\text{physical}}}\right).$$
$$(A2)$$

$\alpha_s(M)$ is the QCD coupling constant evaluated at scale M and the ratio of α_s factors resums leading logarithms in HQET in the decay constant [100]. We take α_s in the $\overline{\text{MS}}$ scheme from lattice QCD [70]. The power p is then $-6/25$ (for $n_f = 4$) for the f_{H_c} fit and $+6/25$ for the fit to the ratio $h_{A_1}^s(1)/(f_{H_c}\sqrt{M_{H_c}})$. The leading power of M_{η_h}, n, is -1 for the fit to f_{H_c} based on HQET expectations, but 0 for the fit to the ratio because we have used $f_{H_c}\sqrt{M_{H_c}}$ in the denominator to remove half-integer powers of ε_h from the fit. The remainder of the fit function allows for inverse powers of m_h and discretization effects. $\mathcal{N}_{\text{mistuning}}$ is the same as that defined earlier for our $h_{A_1}^s$ fit and is given in Eq. (27). The final term allows for c quark mistuning with prior on c_c of 0 ± 1. We take a prior on the overall constant A of 0 ± 4 (GeV$^{3/2}$) in the f_{H_c} fit and 0 ± 2 (GeV$^{-3/2}$) in the ratio fit. Priors on the d_{ijk} are taken as 0 ± 2 except for d_{000} which is defined to have value 1.0.

The fit to the ratio is shown in Fig. 8 and the fit to f_{H_c} in Fig. 9. For the ratio fit χ^2/dof is 0.27 for 12 d.o.f. and for the f_{H_c} fit, 0.53 for 16. Our final result for f_{H_c} at $m_h = m_b$ agrees with a previous HPQCD heavy-HISQ determination on gluon field configurations including $n_f = 2 + 1$ flavors of sea quarks [68] (shown as the red triangle in Fig. 9). Our final result for the ratio $h_{A_1}^s(1)/(f_{H_c}\sqrt{M_{H_c}})$ at $m_h = m_b$ can then be multiplied by our value for f_{B_c} and the square root of the mass of the B_c meson from the particle data tables [46], to give $h_{A_1}^s(1)$. This value is shown as the bottom point in Fig. 5. Figure 8 compares the result from the ratio fit given by the grey band to the value (shown by inverted red triangle) obtained by taking our baseline fit result for $h_{A_1}^s(1)$ from Eq. (33) and calculating from it the value of the ratio $h_{A_1}^s(1)/(f_{H_c}\sqrt{M_{H_c}})$ using our value for f_{B_c} and the experimental M_{B_c}. The agreement is good, showing the consistency of the two different approaches.

[1] J. T. Wei *et al.* (Belle Collaboration), Measurement of the Differential Branching Fraction and Forward-Backward Asymmetry for $B \to K^{(*)}\ell^+\ell^-$, Phys. Rev. Lett. **103,** 171801 (2009).

[2] J. P. Lees *et al.* (*BABAR* Collaboration), Evidence for an Excess of $\bar{B} \to D^{(*)}\tau^-\bar{\nu}_\tau$ Decays, Phys. Rev. Lett. **109,** 101802 (2012).

[3] J. P. Lees *et al.* (*BABAR* Collaboration), Measurement of branching fractions and rate asymmetries in the rare decays $B \to K^{(*)}l^+l^-$, Phys. Rev. D **86,** 032012 (2012).

[4] J. P. Lees *et al.* (*BABAR* Collaboration), Measurement of an excess of $\bar{B} \to D^{(*)}\tau^-\bar{\nu}_\tau$ decays and implications for charged Higgs bosons, Phys. Rev. D **88,** 072012 (2013).

[5] R. Aaij *et al.* (LHCb Collaboration), Differential branching fractions and isospin asymmetries of $B \to K^{(*)}\mu^+\mu^-$ decays, J. High Energy Phys. 06 (2014) 133.

[6] R. Aaij *et al.* (LHCb Collaboration), Test of Lepton Universality Using $B^+ \to K^+\ell^+\ell^-$ Decays, Phys. Rev. Lett. **113,** 151601 (2014).

[7] M. Huschle *et al.* (Belle Collaboration), Measurement of the branching ratio of $\bar{B} \to D^{(*)}\tau^-\bar{\nu}_\tau$ relative to $\bar{B} \to D^{(*)}\ell^-\bar{\nu}_\ell$ decays with hadronic tagging at Belle, Phys. Rev. D **92,** 072014 (2015).

[8] R. Aaij *et al.* (LHCb Collaboration), Angular analysis of the $B^0 \to K^{*0}\mu^+\mu^-$ decay using 3 fb^{-1} of integrated luminosity, J. High Energy Phys. 02 (2016) 104.

[9] R. Aaij *et al.* (LHCb Collaboration), Measurement of the Ratio of Branching Fractions $\mathcal{B}(\bar{B}^0 \to D^{*+}\tau^-\bar{\nu}_\tau)/\mathcal{B}(\bar{B}^0 \to D^{*+}\mu^-\bar{\nu}_\mu)$, Phys. Rev. Lett. **115,** 111803 (2015); Erratum **115,** 159901 (2015).

[10] R. Aaij *et al.* (LHCb Collaboration), Differential branching fraction and angular analysis of $\Lambda_b^0 \to \Lambda\mu^+\mu^-$ decays, J. High Energy Phys. 06 (2015) 115; Erratum 09 (2018) 145.

[11] R. Aaij *et al.* (LHCb Collaboration), Measurements of the S-wave fraction in $B^0 \to K^+\pi^-\mu^+\mu^-$ decays and the $B^0 \to K^*(892)^0\mu^+\mu^-$ differential branching fraction, J. High Energy Phys. 11 (2016) 047; Erratum 04 (2017) 142.

[12] S. Wehle *et al.* (Belle Collaboration), Lepton-Flavor-Dependent Angular Analysis of $B \to K^*\ell^+\ell^-$, Phys. Rev. Lett. **118,** 111801 (2017).

[13] Y. Sato *et al.* (Belle Collaboration), Measurement of the branching ratio of $\bar{B}^0 \to D^{*+}\tau^-\bar{\nu}_\tau$ relative to $\bar{B}^0 \to D^{*+}\ell^-\bar{\nu}_\ell$ decays with a semileptonic tagging method, Phys. Rev. D **94,** 072007 (2016).

[14] S. Hirose *et al.* (Belle Collaboration), Measurement of the τ lepton polarization and $R(D^*)$ in the decay $\bar{B} \to D^*\tau^-\bar{\nu}_\tau$ with one-prong hadronic τ decays at Belle, Phys. Rev. D **97,** 012004 (2018).

[15] R. Aaij *et al.* (LHCb Collaboration), Test of lepton flavor universality by the measurement of the $B^0 \to D^{*-}\tau^+\nu_\tau$ branching fraction using three-prong τ decays, Phys. Rev. D **97,** 072013 (2018).

[16] R. Aaij *et al.* (LHCb Collaboration), Measurement of the Ratio of the $B^0 \to D^{*-}\tau^+\nu_\tau$ and $B^0 \to D^{*-}\mu^+\nu_\mu$ Branching Fractions Using Three-Prong τ-Lepton Decays, Phys. Rev. Lett. **120,** 171802 (2018).

[17] R. Aaij *et al.* (LHCb Collaboration), Test of lepton universality with $B^0 \to K^{*0}\ell^+\ell^-$ decays, J. High Energy Phys. 08 (2017) 055.

[18] A. M. Sirunyan *et al.* (CMS Collaboration), Measurement of angular parameters from the decay $B^0 \to K^{*0}\mu^+\mu^-$ in proton-proton collisions at $\sqrt{s} = 8$ TeV, Phys. Lett. B **781,** 517 (2018).

[19] M. Aaboud *et al.* (ATLAS Collaboration), Angular analysis of $B_d^0 \to K^*\mu^+\mu^-$ decays in pp collisions at $\sqrt{s} = 8$ TeV with the ATLAS detector, J. High Energy Phys. 10 (2018) 047.

[20] Y. Amhis *et al.* (HFLAV Collaboration), Averages of b-hadron, c-hadron, and τ-lepton properties as of summer 2016, Eur. Phys. J. C **77,** 895 (2017).

[21] A. J. Bevan *et al.* (*BABAR* and Belle Collaborations), The physics of the B factories, Eur. Phys. J. C **74,** 3026 (2014).

[22] A. Alberti, P. Gambino, K. J. Healey, and S. Nandi, Precision Determination of the Cabibbo-Kobayashi-Maskawa Element V_{cb}, Phys. Rev. Lett. **114,** 061802 (2015).

[23] H. Schroder, New results on heavy quarks from ARGUS and CLEO in heavy quark physics, in *Proceedings of the 138th WE-Heraeus Seminar, Bad Honnef, Germany, 1994* (1994), pp. 9–22.

[24] D. Bortoletto *et al.* (CLEO Collaboration), Exclusive and Inclusive Decays of B Mesons into $D(s)$ Mesons, Phys. Rev. Lett. **64,** 2117 (1990).

[25] R. Fulton *et al.* (CLEO Collaboration), Exclusive and inclusive semileptonic decays of B mesons to D mesons, Phys. Rev. D **43,** 651 (1991).

[26] H. Albrecht *et al.* (ARGUS Collaboration), Measurement of the decay $B \to D_0^*\ell\bar{\nu}$, Phys. Lett. B **275,** 195 (1992).

[27] B. Barish *et al.* (CLEO Collaboration), Measurement of the $\bar{B} \to D^*\ell\bar{\nu}$ branching fractions and $|V_{cb}|$, Phys. Rev. D **51,** 1014 (1995).

[28] D. Buskulic *et al.* (ALEPH Collaboration), Strange b baryon production and lifetime in Z decays, Phys. Lett. B **384,** 449 (1996).

[29] D. Buskulic *et al.* (ALEPH Collaboration), Heavy quark tagging with leptons in the ALEPH detector, Nucl. Instrum. Methods Phys. Res., Sect. A **346,** 461 (1994).

[30] G. Abbiendi *et al.* (OPAL Collaboration), Measurement of $|V_{cb}|$ using $\bar{B}_0 \to D^{*+}\ell\bar{\nu}$ decays, Phys. Lett. B **482,** 15 (2000).

[31] P. Abreu *et al.* (DELPHI Collaboration), Measurement of V(cb) from the decay process $\bar{B}_0 \to D^{*+}\ell\bar{\nu}$, Phys. Lett. B **510,** 55 (2001).

[32] N. E. Adam *et al.* (CLEO Collaboration), Determination of the $\bar{B} \to D^*\ell\bar{\nu}$ decay width and $|V_{cb}|$, Phys. Rev. D **67,** 032001 (2003).

[33] J. Abdallah *et al.* (DELPHI Collaboration), Measurement of $|V_{cb}|$ using the semileptonic decay $\bar{B}_d^0 \to D^*\ell\bar{\nu}_\ell$, Eur. Phys. J. C **33,** 213 (2004).

[34] B. Aubert *et al.* (*BABAR* Collaboration), Determination of the form-factors for the decay $B^0 \to D^{*-}\ell^+\nu_l$ and of the CKM matrix element $|V_{cb}|$, Phys. Rev. D **77,** 032002 (2008).

[35] B. Aubert *et al.* (*BABAR* Collaboration), Measurement of the Decay $B^- \to D^{*0} e^-\bar{\nu}(e)$, Phys. Rev. Lett. **100,** 231803 (2008).

[36] B. Aubert *et al.* (*BABAR* Collaboration), Measurements of the semileptonic decays $\bar{B} \to D\ell\bar{\nu}$ and $\bar{B} \to D^*\ell\bar{\nu}$ using a global fit to $DX\ell\bar{\nu}$ final states, Phys. Rev. D **79,** 012002 (2009).

[37] W. Dungel *et al.* (Belle Collaboration), Measurement of the form factors of the decay $B^0 \to D^{*-}\ell^+\nu$ and determination of the CKM matrix element $|V_{cb}|$, Phys. Rev. D **82,** 112007 (2010).

[38] A. Abdesselam *et al.* (Belle Collaboration), Precise determination of the CKM matrix element $|V_{cb}|$ with $\bar{B}^0 \to D^{*+}\ell^-\bar{\nu}_\ell$ decays with hadronic tagging at Belle, arXiv:1702.01521.

[39] J. A. Bailey *et al.* (Fermilab Lattice and MILC Collaborations), Update of $|V_{cb}|$ from the $\bar{B} \to D^*\ell\bar{\nu}$ form factor at zero recoil with three-flavor lattice QCD, Phys. Rev. D **89,** 114504 (2014).

[40] A. Abdesselam *et al.* (Belle Collaboration), Measurement of CKM matrix element $|V_{cb}|$ from $\bar{B} \to D^{*+}\ell^-\bar{\nu}_\ell$, arXiv:1809.03290.

[41] J. Harrison, C. Davies, and M. Wingate (HPQCD Collaboration), Lattice QCD calculation of the $B_{(s)} \to D^*_{(s)}\ell\nu$ form factors at zero recoil and implications for $|V_{cb}|$, Phys. Rev. D **97,** 054502 (2018).

[42] J. A. Bailey, S. Lee, W. Lee, J. Leem, and S. Park, Updated evaluation of ε_K in the standard model with lattice QCD inputs, Phys. Rev. D **98,** 094505 (2018).

[43] F. U. Bernlochner, Z. Ligeti, M. Papucci, and D. J. Robinson, Combined analysis of semileptonic B decays to D and D^*: $R(D^{(*)})$, $|V_{cb}|$, and new physics, Phys. Rev. D **95,** 115008 (2017); Erratum **97,** 059902 (2018).

[44] D. Bigi, P. Gambino, and S. Schacht, A fresh look at the determination of $|V_{cb}|$ from $B \to D^*\ell\nu$, Phys. Lett. B **769,** 441 (2017).

[45] B. Grinstein and A. Kobach, Model-independent extraction of $|V_{cb}|$ from $\bar{B} \to D^*\ell\bar{\nu}$, Phys. Lett. B **771,** 359 (2017).

[46] M. Tanabashi *et al.* (Particle Data Group), Review of particle physics, Phys. Rev. D **98,** 030001 (2018).

[47] J. P. Lees *et al.* (BABAR Collaboration), A test of heavy quark effective theory using a four-dimensional angular analysis of $\bar{B} \to D^*\ell^-\bar{\nu}_\ell$, arXiv:1903.10002 [Phys. Rev. Lett (to be published)].

[48] G. Caria (Belle Collaboration), Measurement of $R(D)$ and $R(D^*)$ with a semileptonic tag at Belle, in *Proceedings of 54th Rencontres de Moriond on Electroweak Interactions, 2019, La Thuile, Italy* (2019).

[49] G. C. Donald, C. T. H. Davies, J. Koponen, and G. P. Lepage (HPQCD Collaboration), Prediction of the D^*_s Width from a Calculation of its Radiative Decay in Full Lattice QCD, Phys. Rev. Lett. **112,** 212002 (2014).

[50] J. A. Bailey *et al.* (Fermilab/MILC Collaborations), $B_s \to D_s/B \to D$ Semileptonic form-factor ratios and their application to BR$(B_s^0 \to \mu^+\mu^-)$, Phys. Rev. D **85,** 114502 (2012); Erratum **86,** 039904 (2012).

[51] J. Koponen, C. T. H. Davies, G. C. Donald, E. Follana, G. P. Lepage, H. Na, and J. Shigemitsu (HPQCD Collaboration), The shape of the $D \to K$ semileptonic form factor from full lattice QCD and V_{cs}, arXiv:1305.1462.

[52] C. J. Monahan, H. Na, C. M. Bouchard, G. P. Lepage, and J. Shigemitsu (HPQCD Collaboration), $B_s \to D_s\ell\nu$ Form factors and the fragmentation fraction ratio f_s/f_d, Phys. Rev. D **95,** 114506 (2017).

[53] E. E. Jenkins and M. J. Savage, Light quark dependence of the Isgur-Wise function, Phys. Lett. B **281,** 331 (1992).

[54] C. Bernard *et al.* (Fermilab/MILC Collaborations), The $\bar{B} \to D^*\ell\bar{\nu}$ form factor at zero recoil from three-flavor lattice QCD: A Model independent determination of $|V_{cb}|$, Phys. Rev. D **79,** 014506 (2009).

[55] A. X. El-Khadra, A. S. Kronfeld, and P. B. Mackenzie, Massive fermions in lattice gauge theory, Phys. Rev. D **55,** 3933 (1997).

[56] A. Bazavov *et al.* (MILC Collaboration), Nonperturbative QCD simulations with 2+1 flavors of improved staggered quarks, Rev. Mod. Phys. **82,** 1349 (2010).

[57] G. P. Lepage, L. Magnea, C. Nakhleh, U. Magnea, and K. Hornbostel, Improved nonrelativistic QCD for heavy quark physics, Phys. Rev. D **46,** 4052 (1992),

[58] R. J. Dowdall *et al.* (HPQCD Collaboration), The Upsilon spectrum and the determination of the lattice spacing from lattice QCD including charm quarks in the sea, Phys. Rev. D **85,** 054509 (2012).

[59] E. Follana, Q. Mason, C. Davies, K. Hornbostel, G. P. Lepage, J. Shigemitsu, H. Trottier, and K. Wong (HPQCD and UKQCD Collaborations), Highly improved staggered quarks on the lattice, with applications to charm physics, Phys. Rev. D **75,** 054502 (2007).

[60] J. Flynn, T. Izubuchi, A. Juttner, T. Kawanai, C. Lehner, E. Lizarazo, A. Soni, J. T. Tsang, and O. Witzel, Form factors for semi-leptonic B decays, Proc. Sci., LATTICE2016 (**2016**) 296 [arXiv:1612.05112].

[61] J. A. Bailey, T. Bhattacharya, R. Gupta, Y.-C. Jang, W. Lee, J. Leem, S. Park, and B. Yoon (LANL-SWME Collaboration), Calculation of $\bar{B} \to D^*\ell\bar{\nu}$ form factor at zero recoil using the Oktay-Kronfeld action, EPJ Web Conf. **175,** 13012 (2018).

[62] T. Kaneko, Y. Aoki, B. Colquhoun, H. Fukaya, and S. Hashimoto (JLQCD Collaboration), $B \to D^{(*)}\ell\nu$ form factors from $N_f = 2 + 1$ QCD with Möbius domain-wall quarks, Proc. Sci. LATTICE2018 (**2018**) 311 [arXiv:1811.00794]

[63] J. Harada, S. Hashimoto, A. S. Kronfeld, and T. Onogi, Application of heavy quark effective theory to lattice QCD. 3. Radiative corrections to heavy-heavy currents, Phys. Rev. D **65,** 094514 (2002).

[64] C. Monahan, J. Shigemitsu, and R. Horgan, Matching lattice and continuum axial-vector and vector currents with nonrelativistic QCD and highly improved staggered quarks, Phys. Rev. D **87,** 034017 (2013).

[65] A. Bazavov *et al.* (MILC Collaboration), Scaling studies of QCD with the dynamical HISQ action, Phys. Rev. D **82,** 074501 (2010).

[66] A. Bazavov *et al.* (MILC Collaboration), Lattice QCD ensembles with four flavors of highly improved staggered quarks, Phys. Rev. D **87,** 054505 (2013).

[67] C. McNeile, C. T. H. Davies, E. Follana, K. Hornbostel, and G. P. Lepage (HPQCD Collaboration), High-precision f_{B_s} and HQET from relativistic lattice QCD, Phys. Rev. D **85,** 031503 (2012).

[68] C. McNeile, C. T. H. Davies, E. Follana, K. Hornbostel, and G. P. Lepage, Heavy meson masses and decay constants from relativistic heavy quarks in full lattice QCD, Phys. Rev. D **86,** 074503 (2012).

[69] C. McNeile, C. T. H. Davies, E. Follana, K. Hornbostel, and G. P. Lepage, High-precision c and b masses, and QCD

coupling from current-current correlators in lattice and continuum QCD, Phys. Rev. D **82**, 034512 (2010).

[70] B. Chakraborty, C. T. H. Davies, B. Galloway, P. Knecht, J. Koponen, G. C. Donald, R. J. Dowdall, G. P. Lepage, and C. McNeile (HPQCD), High-precision quark masses and QCD coupling from $n_f = 4$ lattice QCD, Phys. Rev. D **91**, 054508 (2015).

[71] A. Bazavov *et al.* (Fermilab/MILC), *B*- and *D*-meson leptonic decay constants from four-flavor lattice QCD, Phys. Rev. D **98**, 074512 (2018).

[72] P. Petreczky and J. H. Weber, Strong coupling constant and heavy quark masses in 2+1 flavor QCD, arXiv: 1901.06424.

[73] A. Lytle, B. Colquhoun, C. Davies, J. Koponen, and C. McNeile (HPQCD), Semileptonic B_c decays from full lattice QCD, Proc. Sci., BEAUTY2016 (**2016**) 069 [arXiv:1605.05645].

[74] B. Colquhoun, C. Davies, J. Koponen, A. Lytle, and C. McNeile (HPQCD), B_c decays from highly improved staggered quarks and NRQCD, Proc. Sci., LATTICE2016 (**2016**) 281 [arXiv:1611.01987].

[75] A. Sirlin, Large m(W), m(Z) behavior of the O(alpha) corrections to semileptonic processes mediated by W, Nucl. Phys. **B196**, 83 (1982).

[76] E. S. Ginsberg, Radiative corrections to k-e-3-neutral decays and the delta-i=1/2 rule, Phys. Rev. **171**, 1675 (1968); Erratum **174**, 2169 (1968).

[77] D. Atwood and W. J. Marciano, Radiative corrections and semileptonic *B* decays, Phys. Rev. D **41**, 1736 (1990).

[78] J. D. Richman and P. R. Burchat, Leptonic and semileptonic decays of charm and bottom hadrons, Rev. Mod. Phys. **67**, 893 (1995).

[79] A. Hart, G. M. von Hippel, and R. R. Horgan (HPQCD Collaboration), Radiative corrections to the lattice gluon action for HISQ improved staggered quarks and the effect of such corrections on the static potential, Phys. Rev. D **79**, 074008 (2009).

[80] B. Chakraborty, C. T. H. Davies, P. G. de Oliviera, J. Koponen, G. P. Lepage, and R. S. Van de Water (HPQCD Collaboration), The hadronic vacuum polarization contribution to a_μ from full lattice QCD, Phys. Rev. D **96**, 034516 (2017).

[81] C. McNeile (private communication).

[82] R. J. Dowdall, C. T. H. Davies, G. P. Lepage, and C. McNeile (HPQCD Collaboration), Vus from pi and K decay constants in full lattice QCD with physical u, d, s and c quarks, Phys. Rev. D **88**, 074504 (2013).

[83] C. T. H. Davies, E. Follana, I. D. Kendall, G. P. Lepage, and C. McNeile (HPQCD Collaboration), Precise determination of the lattice spacing in full lattice QCD, Phys. Rev. D **81**, 034506 (2010).

[84] G. C. Donald, C. T. H. Davies, J. Koponen, and G. P. Lepage (HPQCD Collaboration), V_{cs} from $D_s \to \phi\ell\nu$ semileptonic decay and full lattice QCD, Phys. Rev. D **90**, 074506 (2014).

[85] G. P. Lepage, B. Clark, C. T. H. Davies, K. Hornbostel, P. B. Mackenzie, C. Morningstar, and H. Trottier, Constrained curve fitting, Nucl. Phys. B, Proc. Suppl. **106**, 12 (2002).

[86] Corrfitter, https://github.com/gplepage/corrfitter (2018).

[87] C. T. H. Davies, C. McNeile, E. Follana, G. P. Lepage, H. Na, and J. Shigemitsu (HPQCD Collaboration), Corrfitter, Phys. Rev. D **82**, 114504 (2010).

[88] S. Naik, On-shell improved lattice action for QCD with Susskind fermions and asymptotic freedom scale, Nucl. Phys. **B316**, 238 (1989).

[89] M. E. Luke, Effects of subleading operators in the heavy quark effective theory, Phys. Lett. B **252**, 447 (1990).

[90] A. F. Falk and M. Neubert, Second order power corrections in the heavy quark effective theory. 1. Formalism and meson form-factors, Phys. Rev. D **47**, 2965 (1993).

[91] T. Mannel, Higher order 1/m corrections at zero recoil, Phys. Rev. D **50**, 428 (1994).

[92] A. Czarnecki, Two Loop QCD Corrections to b –> c Transitions at Zero Recoil, Phys. Rev. Lett. **76**, 4124 (1996).

[93] F. E. Close, G. J. Gounaris, and J. E. Paschalis, The ratio $\gamma(B \to D\ell$ neutrino) / $\gamma(B \to D^*\ell$ neutrino) in the quark model, Phys. Lett. **149B**, 209 (1984).

[94] A. Bazavov *et al.* (Fermilab Lattice, MILC, and TUMQCD Collaborations), Up-, down-, strange-, charm-, and bottom-quark masses from four-flavor lattice QCD, Phys. Rev. D **98**, 054517 (2018).

[95] N. Brambilla, J. Komijani, A. S. Kronfeld, and A. Vairo (TUMQCD Collaboration), Relations between heavy-light meson and quark masses, Phys. Rev. D **97**, 034503 (2018).

[96] J. Laiho and R. S. Van de Water, $B \to D^*\ell\nu$ and $B \to D\ell\nu$ form factors in staggered chiral perturbation theory, Phys. Rev. D **73**, 054501 (2006).

[97] C. Bernard and D. Toussaint (MILC Collaboration), Effects of nonequilibrated topological charge distributions on pseudoscalar meson masses and decay constants, Phys. Rev. D **97**, 074502 (2018).

[98] A. V. Avilés-Casco, C. DeTar, A. X. El-Khadra, A. S. Kronfeld, J. Laiho, and R. S. Van de Water, $B \to D^*\ell\nu$ at non-zero recoil, Proc. Sci. LATTICE2018 (**2018**) 282 [arXiv:1901.00216].

[99] E. McLean, C. T. H. Davies, A. T. Lytle, and J. Koponen (HPQCD Collaboration), $B_s \to D_s^{(*)}l\nu$ Form factors with heavy HISQ quarks, Proc. Sci. LATTICE2018 (**2018**) 281 [arXiv:1901.04979].

[100] M. Neubert, Heavy quark symmetry, Phys. Rep. **245**, 259 (1994).